INTERACTION NOTES

NOTE 232

November 1970

Measurements of and Discrimination with Smoothed Impulse Responses of Radar Targets

Robert S. Smith
Joseph D. DeLorenzo
C. Leonard Bennett

Sperry Rand Research Center

ABSTRACT

One of the more pressing problems in the application of radar technology is the extraction of a maximum amount of information from the backscattered fields of various types of radar targets to permit their classification and identification. It is axiomatic that very wideband signals are required to achieve this objective, and a number of investigators have attempted to use, with partial success, wideband radar signals to construct visually recognizable images of relatively large radar reflectors. In this study we describe an alternate system concept based primarily on the use of a bank of digital matched filters matched to the scattered-field responses in the resonance region of targets of interest. Supporting laboratory data and computer simulation results show that this approach can be an effective means of accurately discriminating among targets of similar size and shape, or among the different physical orientations of the same target, even when such targets are obscured by noise or clutter.

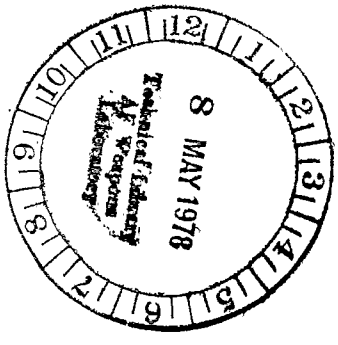

TABLE OF CONTENTS

LIST OF ILLUSTRATIONS

LIST OF ILLUSTRATIONS (cont.)

SECTION 1

INTRODUCTION

This document is submitted as the final report in response to the requirements set forth in Contract No. F30602-69-C-0357 between the Sperry Rand Research Center, Sudbury, Massachusetts and the Air Force Systems Command, Rome Air Development Center, Griffiss Air Force Base, New York. The primary objective of this program, performed during the period 22 June 1969 to 22 June 1970, was to obtain and analyze the impulse response measurements of five satellite-type objects. In particular, the main task was to determine or obtain a quantitative measure of the target discriminants that exist in the electromagnetic field backscattered from these bodies.

The motivation for this study is based on the fact that broadband radars with sophisticated signal processors are being proposed as solutions to both clutter and object identification problems. While many fine studies leading to such proposals have been made, lack of knowledge of the scattering characteristics, valid over a large enough frequency band to satisfy system requirements, has prevented the design of truly optimum processors for target discrimination.

Recent advances in the application of picosecond technology to microwave problems have led to the development of a scattering facility that can provide accurate measurements of the smoothed impulse response of the scattering object.

One advantage of this approach to gathering target data is that it takes only a few minutes to demonstrate that scattering objects with different shapes have different impulse responses. This led to the decision to use these characteristic signatures as input data for a signal processing scheme to identify specific targets. In addition, the impulse response waveform is simple enough in structure to permit us to employ a laboratory instrumentation computer to process the data.

The operating band of the system presently covers the range from 200 MHz to about 4.5 GHz. We should note, however, that as long as the width of the smoothed impulse is short enough to resolve (in a radar sense) the

pertinent target details, then both high- and low-frequency effects are contained in this smoothed impulse-response waveform. Increasing the high-frequency content by decreasing the pulse width will simply sharpen the response without furnishing additional useful information about the target. In the frequency domain, this amounts to saying that the useful information is contained in the baseband extending to a frequency somewhat above the highest significiant resonance.

The approach taken in this study to obtain a measure of existing discriminants among different scatterers was to measure the response of these objects on the time-domain scattering range and then compute the elements of the cross-correlation matrix. In order to show the effects of bandlimiting on these discriminants, the measured returns were filtered and the correlation matrix was recomputed. These data quantitatively measure the waveform differences; however, in order to obtain a measure of performance of a target identification system using these responses, noise must be introduced into the system. A theoretical derivation of optimum discrimination systems employing these smoothed impulse response waveforms was carried out for several potential system environments. These optimum discriminators were implemented in the time-domain metrology laboratory and tested with the measured waveforms. The results of these tests indicate that targets can be effectively identified on the basis of their impulse response. It should be noted that a currently active Air Force project, SPERT, to develop the necessary technology to implement a high percent bandwidth radar can employ many of the concepts and results presented here.

The next section of this paper presents a brief description of the precision time-domain scattering facility along with a discussion of some scattering results that are pertinent to the signal processing aspects of our study. In Sec. 3 the digital signal processing philosophy that was used to quantitatively measure target discriminants is discussed. The resulting correlation matrices under various bandwidth constraints are also discussed. Section 4 presents the thoeretical derivations of several optimum discriminators, while in Sec. 5 the digital implementation of the discriminators and the experimental results obtained in the time-domain metrology laboratory are discussed. Section 6 is a summary of the reported results.

SECTION 2

TARGET MEASUREMENTS

The electromagnetic response of a radar target contains all the scattering information about that target, and for this reason is a characteristic target signature. Moreover, the impulse response displays this enormous amount of information in a deceptively simple waveform which is also closely related to the actual target geometry. Section 2.1 discusses the time-domain scattering range facility which provides a quantitatively accurate means of measuring the smoothed impulse responses of radar targets. Results are then presented and discussed (including the relationship between characteristics of the smoothed impulse response and the target geometry) in Sec. 2.2.

2.1 SCATTERING RANGE DESCRIPTION

The operating principles of the scattering range are most easily understood by considering the functional block diagram shown in Fig. 1. The system signal source is a high-voltage switch which generates a 300 V step function with a risetime less than 100 psec. The signal is radiated, virtually undistorted, from the base of a wire transmitting antenna protruding through a circular ground plane 20 feet in diameter. This wave is then reflected by a target and the scattered waveform is received on a coaxial horn antenna, which essentially differentiates the signal and thus provides the impulse response of the target. The received waveform is sampled by a 12 GHz oscilloscope that has been triggered by the initial pulse and whose sampling gate deflection is under the control of a small instrumentation computer. Unprocessed data are displayed on the osciloscope CRT while the sampled-and-held waveform is passed through a low-pass filter, digitized, read into the computer, and stored on magnetic tape automatically. This system has been designed to correct for long-term timing drift and/or amplifier drift. In addition, the waveforms are stored in such a way that they are ready for the subsequent operations of averaging (to remove short-term noise) and baseline processing.*

* The effects of a time varying baseline are subtracted from measured waveforms to improve system accuracy.

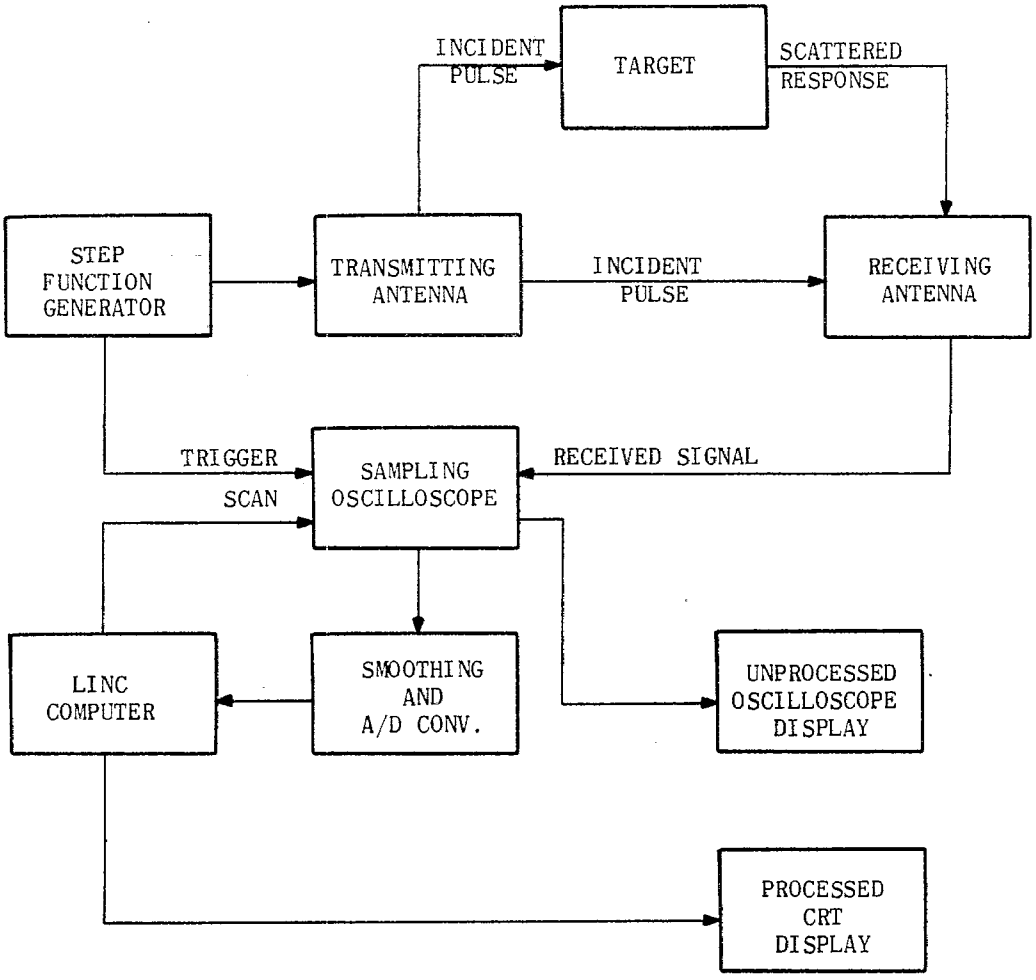

FIG. 1 Functional block diagram of video time-domain scattering range.

The salient characteristics of the range are the speed and simplicity with which multi-octave frequency-domain data can be obtained. These advantages accrue because the time-domain scattering range yields an "uncontaminated" interval of time between the arrival of the direct wave and the arrival of unwanted reflections. This is most easily explained by considering the sketch in Fig. 2, which shows the relative location of the elements on the ground plane, and the photographs in Fig. 3, which show the range response as it appears at the oscilloscope (no data processing has been used at this point). The transmitted signal travels outward from the base of the wire antenna and is received at R at time $t_0 = \frac{d}{c}$ (where c is the speed of light). This time is marked by the pulse at the left end of the trace in Fig. 3. The outgoing wave reaches the target at $t = \frac{r}{c}$, is reflected, and arrives at the receiver at $t_1 = \frac{2r+d}{c} = t_0 + \frac{2r}{c}$. The targets are usually located anywhere from 2 to 5 feet from the transmitting antenna; therefore, target returns lie in the region marked by the doublets at t_1 and t_2 in the lower photograph. The erratic response at the right edge of the trace which occurs after t_3 marks the arrival of the pulse reflected by the table edge and the effects of the pulse radiated from the tip of the transmitting antenna. It should be noted that a "clear window" exists between the second doublet and the table edge. This is required because many of the targets are highly dispersive and their response will extend far beyond the specular reflection (e.g., see Fig. 7). The entire region between the direct transmission and the table edge response forms a convenient time "window" to view the target response and allows one to "gate out" (in time) unwanted reflections. Thus, undistorted transient target responses can be viewed without resorting to elaborate and expensive anechoic chambers. In addition, a single time-domain measurement obviates the requirement for tedious measurement of the amplitude and phase response at many frequencies.

2.2 MEASURED RESULTS

The feasibility of accurately measuring the smoothed impulse response on the time-domain scattering range has been demonstrated quantitatively. In the results that follow, the sampled data from the oscilloscope have been smoothed and the contamination of the baseline has been removed to give the approximate impulse response.

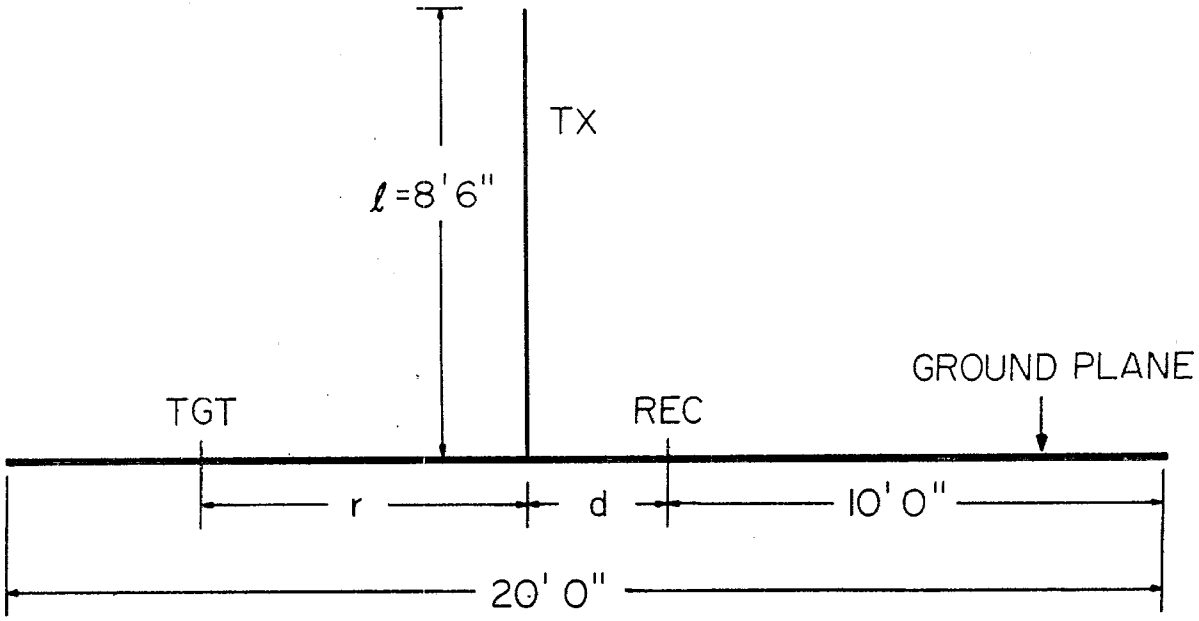

FIG. 2 Geometrical configuration of video time-domain scattering range.

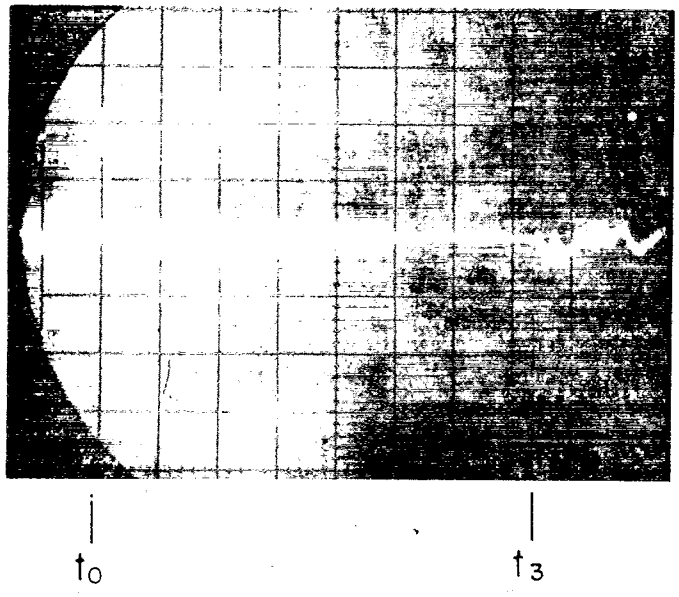

Incident pulse with clear range

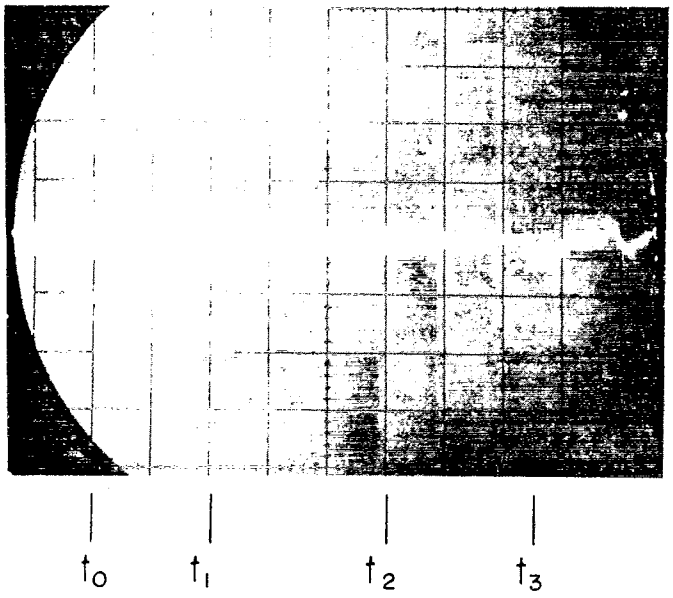

Incident pulse with markers at 2 ft. (t_1) and at 5 ft. (t_2) from transmitting antenna.

FIG. 3 Response of video time-domain scattering range showing incident pulse and time window (horizontal scale: 2 nsec/div.; vertical scale: 200 mV/div.).

The measured incident pulse is shown in Fig. 4 along with the incident pulse used for the theoretical time-domain calculations. The measured response of a 4.25 in. diameter sphere in the backscatter direction is shown in Fig. 5 along with the theoretical results. The agreement between these results is excellent. The initial pulse in the response corresponds to the return from the nose of the sphere (the specular return). The amplitude of this initial return is proportional to the square root of the product of the major radii of curvature at the specular point. Next, a negative swing occurs in the response. The character of this negative swing is influenced only by the shape of the target in the vicinity of the specular point. The timing of the second positive pulse in the response indicates it is due to a wave "traveling" around the rear of the sphere (often called the creeping wave). These results illustrate the close relationship between the approximate impulse response and the geometry of the scatterer.

To demonstrate the utility of time-domain scattering measurements for obtaining broadband frequency response data and at the same time demonstrate the accuracy of the measurements, the frequency response of the sphere has been calculated from the Fourier transforms of the measured incident pulse and the resulting scattered response. The Fourier transforms were performed numerically on a digital computer using a finite Fourier transform approximation for the infinite Fourier transform. In Fig. 6 the result obtained from the measured data displayed in Figs. 4 and 5 is compared with the theoretical frequency response of the sphere calculated with classical techniques. The agreement is quite good up to a ka of approximately 4. The range of good agreement is limited primarily by the spectral content of the incident pulse and could be extended by using larger targets and/or shorter pulses.

The accuracy of the measurement system can be estimated by realizing that the situation that prevails is essentially the same as the elementary statistical problem of estimating the mean V_m of a random variable V when given N independent sample values V_i. In our case the signal voltage is V_m, the signal plus noise is the random variable V, and the expected value of the noise voltage is zero. We therefore use the sample mean

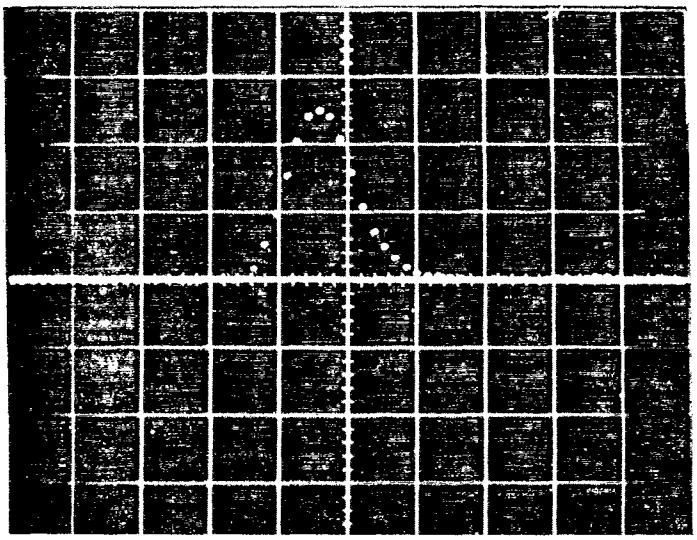

Measured incident pulse

(horiz. scale approx. one sphere radius/div.)

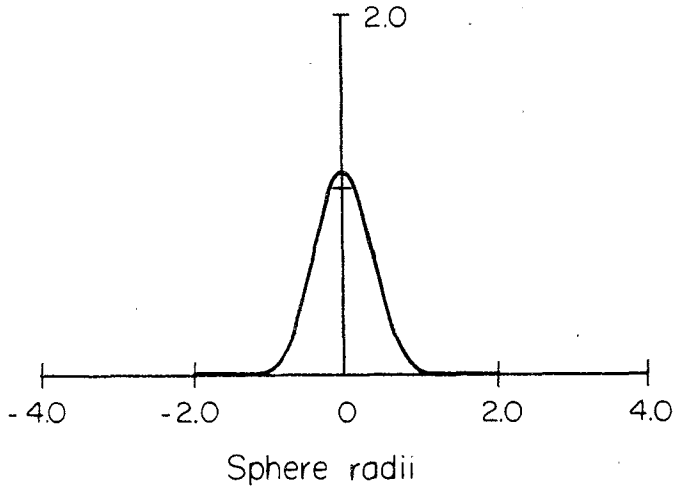

Incident pulse used for theoretical calculation

FIG. 4 Comparison of measured and theoretical incident pulse.

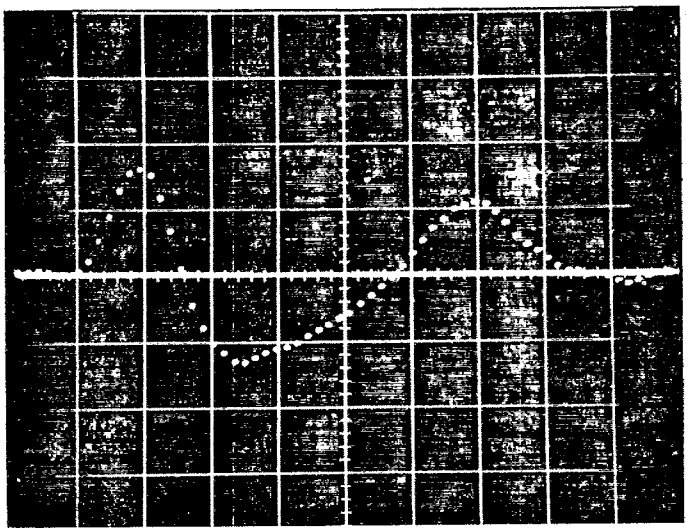

Measured sphere response

(Horizontal scale approximately one sphere radius per div.)

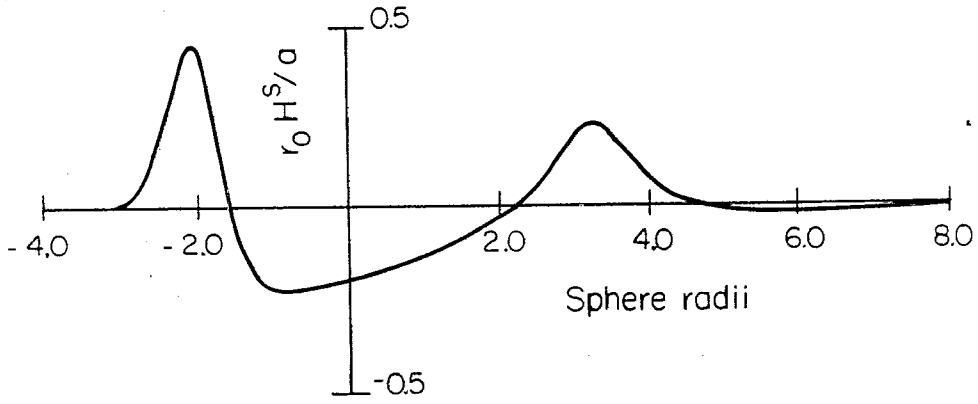

Theoretical response of sphere with radius a

FIG. 5 Comparison of measured and theoretical time-domain sphere response.

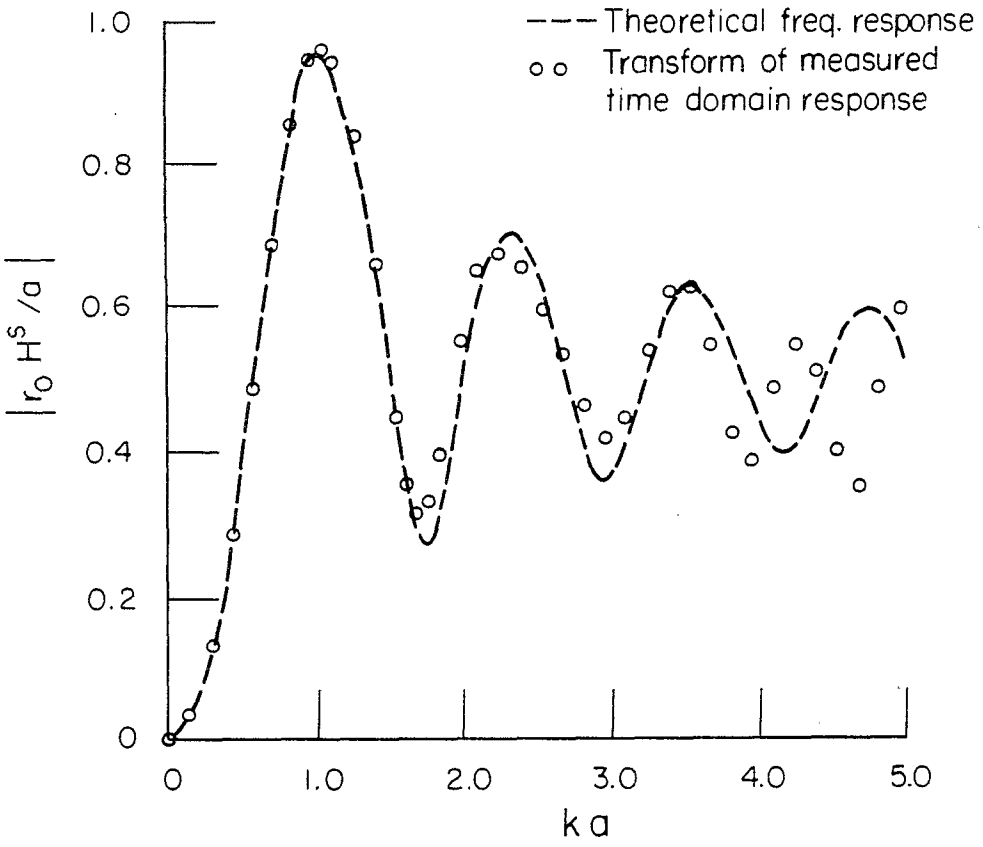

FIG. 6 Backscatter frequency response of sphere with radius a .

$$\bar{V} = \frac{\sum_{i=1}^{N} V_i}{N}$$

as an estimator for V_m (the signal value at a particular point t on the sampled waveform) since it is consistent and unbiased. We take as an error estimate the standard deviation of $\bar{V}$

$$\sigma_{\bar{V}} \approx \frac{S}{\sqrt{N}}$$

which is computed using the sample variance

$$S^2 = \frac{\sum_{i=1}^{N} (V_i - \bar{V})^2}{N}$$

as an estimate for the population variance.

In our measurements the peak of the incident pulse, as measured on the sampling oscilloscope, is approximately 500 mV, and a typical target response has a peak value in the vicinity of 10 mV. When using the 10 mV scale on the sampling oscilloscope, we estimate the standard deviation of $\bar{V}$, as described in the preceding paragraph, to be

$$\sigma_{\bar{V}} = 0.059 \text{ mV}$$

if $N=64$ scans are averaged. Thus, the estimated standard deviation of $\bar{V}$ is in the vicinity of 0.6% of the peak value of the target response.

The previous paragraphs have described the operation of the time-domain scattering range and presented results which show quantitative agreement with previously obtained data for the conducting sphere. Numerous other examples of the good agreement between time-domain scattering range measurements and the results of solving the space-time integral equation are presented elsewhere.[1] The results of the measurements on a cube, a right square cylinder, a right circular cylinder, two spheres, a sphere-capped circular cylinder, and a sphere-cone-sphere are now presented.

In Fig. 7 the smoothed impulse response (in the backscatter direction) of an 8 in. cube is shown for two angles of incidence. For 0° incidence the return from the front face takes the form of a smoothed doublet, as expected. Next the response becomes small, indicating little return from the sides of the cube, and approximately 1.4 nsec after the smoothed doublet there appears a negative pulse whose timing can be attributed to the back edge of the cube. For 45° incidence the first part of the response is a positive pulse that may be attributed to the front vertical edge of the cube. This is followed approximately 0.9 nsec later by a return that may be attributed to the two middle vertical edges. The return due to a wave traveling around the rear of the cube at the speed of light would be expected 2.5 nsec after the return from the front edge, and indeed the measured response does show a pulse approximately 2.7 nsec after the initial pulse.

In Fig. 8 the smoothed impulse response of a right square cylinder that was 12 in. long and 4 in. square is shown for various angles of incidence. For 0° incidence the first portion of the return approximates a doublet and is followed by a negligible return from the sides of the cylinder. The return from the rear edge of the cylinder appears approximately 2.1 nsec later and is followed by the return due to the wave traveling around the rear(a positive pulse at 2.5 nsec). These two returns, when combined, are "doublet-like" in shape, but are of opposite polarity from the return from the front face. This change of polarity would produce a 180° phase shift if convolved with a sinusoidal waveform. At 30° and 60° incidence the doublet character of the initial return and the back return disappears, but the waveform features can again be

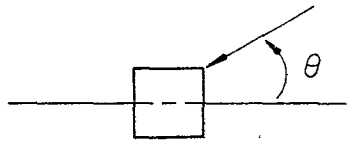

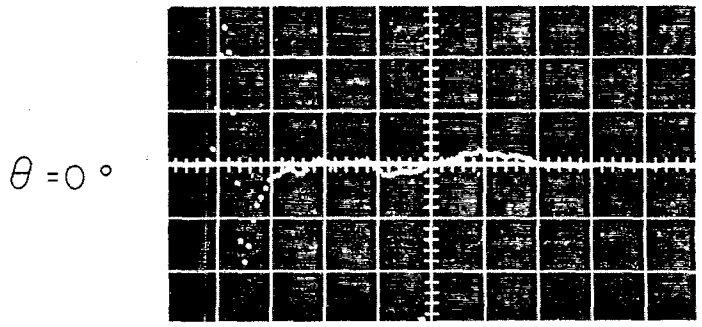

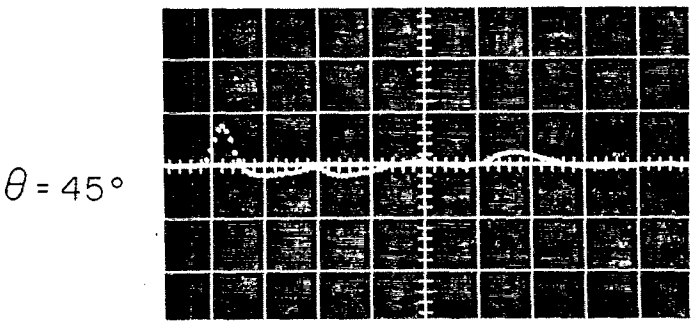

FIG. 7 Smoothed impulse response of an 8 in. cube (horizontal scale: 0.5 nsec/div., vertical scale: 10 mV/div.).

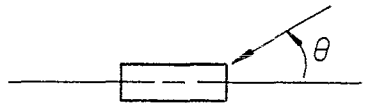

θ = 0°

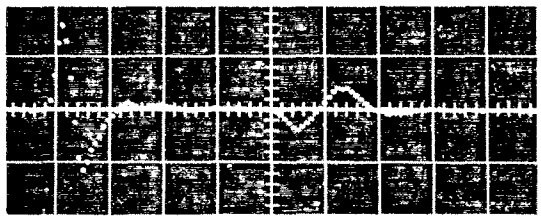

θ = 30°

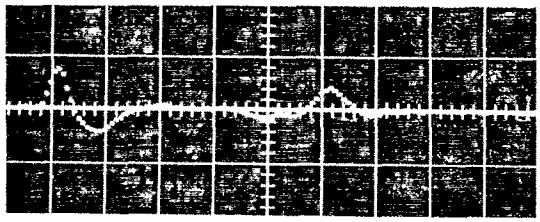

θ = 60°

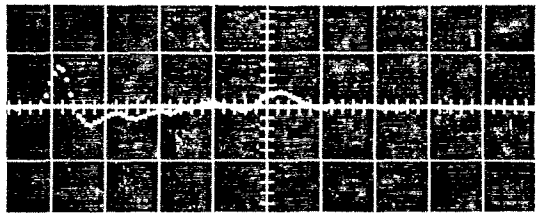

θ = 90°

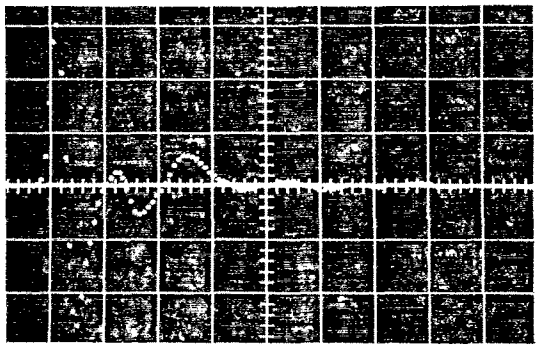

FIG. 8 Smoothed impulse response of a right square cylinder (horizontal scale: 0.5 nsec/div.; vertical scale: 5 mV/div.).

attributed to various geometric features of the target. Finally, at 90^{o} incidence the large doublet return from the side face of the square cylinder appears and is followed by returns due to the back side (a negative pulse at 0.65 nsec) and a wave traveling around the rear (a positive pulse at 1.1 nsec).

The smoothed impulse response of a right circular cylinder that was 12 in. long and 4 in. in diameter is displayed in Fig. 9 for several angles of incidence. For 0^{o} incidence the response is nearly the same as that measured for the right square cylinder. The main difference is that the amplitude of the initial doublet is slightly smaller for the circular cylinder, as expected because the cross-sectional area of the circular cylinder is smaller. At 30^{o} and 60^{o} incidence, slight differences in the responses from the two cases appear, but the gross features again may be related to the actual geometry. At 90^{o} incidence, however, the return from the right circular cylinder is markedly different from the right square cylinder. The initial part of the circular cylinder return at 90^{o} incidence approximates an impulse and is followed by a negative swing, as predicted by physical optics. The second positive pulse that appears approximately 2.0 nsec after the first pulse may be attributed to a wave traveling around the rear of the cylinder. Comparison of this measured response with the smoothed impulse response from an infinitely long circular cylinder with TE polarization[2] shows remarkable similarity, and indicates the effect of the ends on a finite cylinder for this polarization of the incident wave is small. This effect has been rigorously discussed by DeLorenzo[3].

In Fig. 10 the smoothed impulse responses of a 4 in. diameter sphere and an 8 in. diameter sphere are shown. These will be used for comparison with the responses of the sphere-capped cylinder and sphere-cone-sphere.

The smoothed impulse response of a sphere-capped cylinder with a length of 12 in. and a diameter of 4 in. is shown in Fig. 11 for various angles of incidence. For 0^{o} incidence the initial part of the return is, as expected, identical to the return from the 4 in. diameter sphere shown in Fig. 10(a). This is followed by a near zero signal, indicating that there is little return from the sides of the cylinder. Finally, the return from the joint between the cylinder and the sphere cap appears, along with the return due to the wave

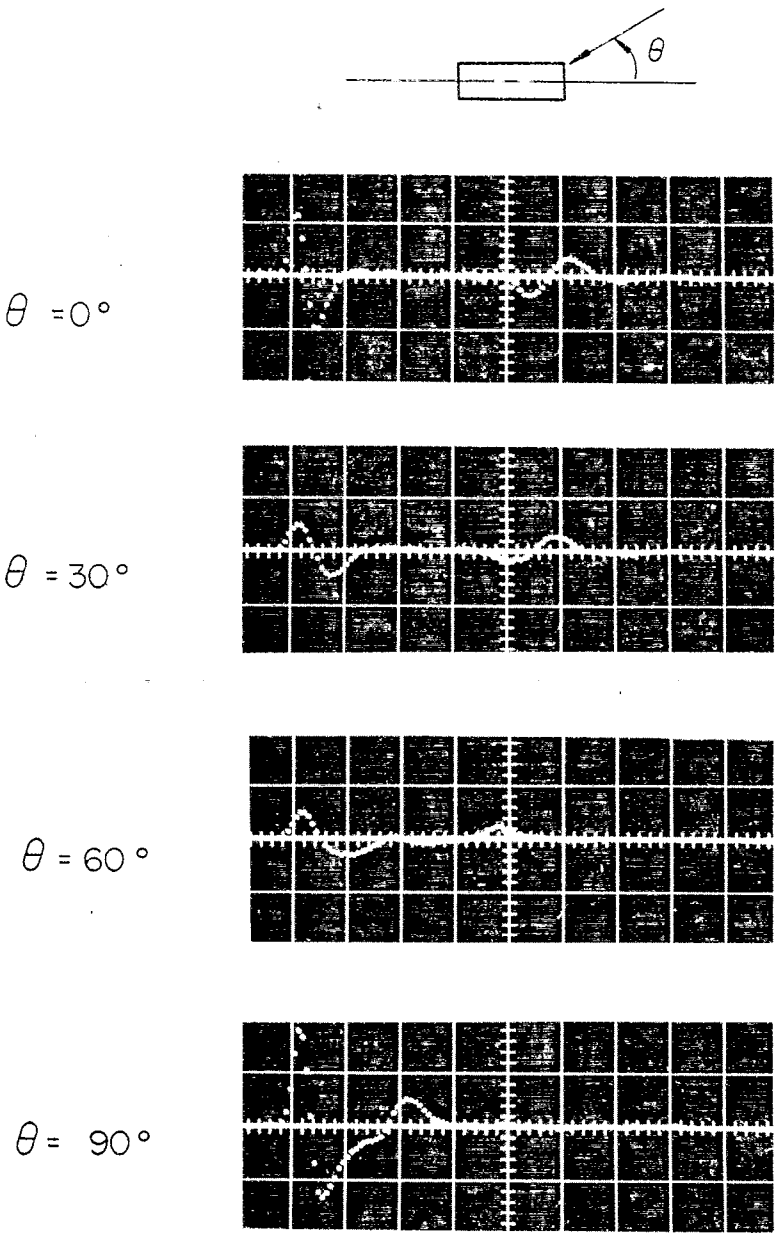

FIG. 9 Smoothed impulse response of a right circular cylinder (horizontal scale: 0.5 nsec/div.; vertical scale: 5 mV/div.).

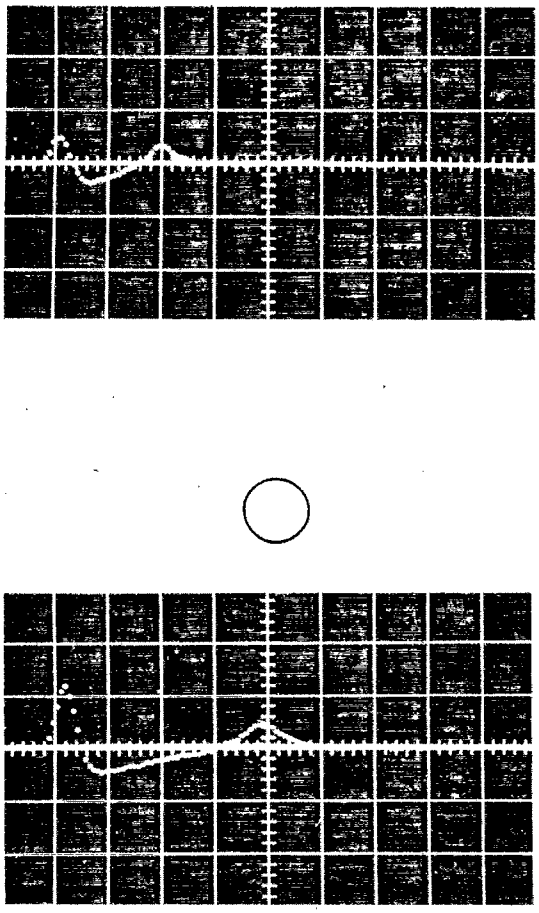

FIG. 10 Smoothed impulse response of spheres (horizontal scale: 0.5 nsec/div.; vertical scale: 5 mV/div.).

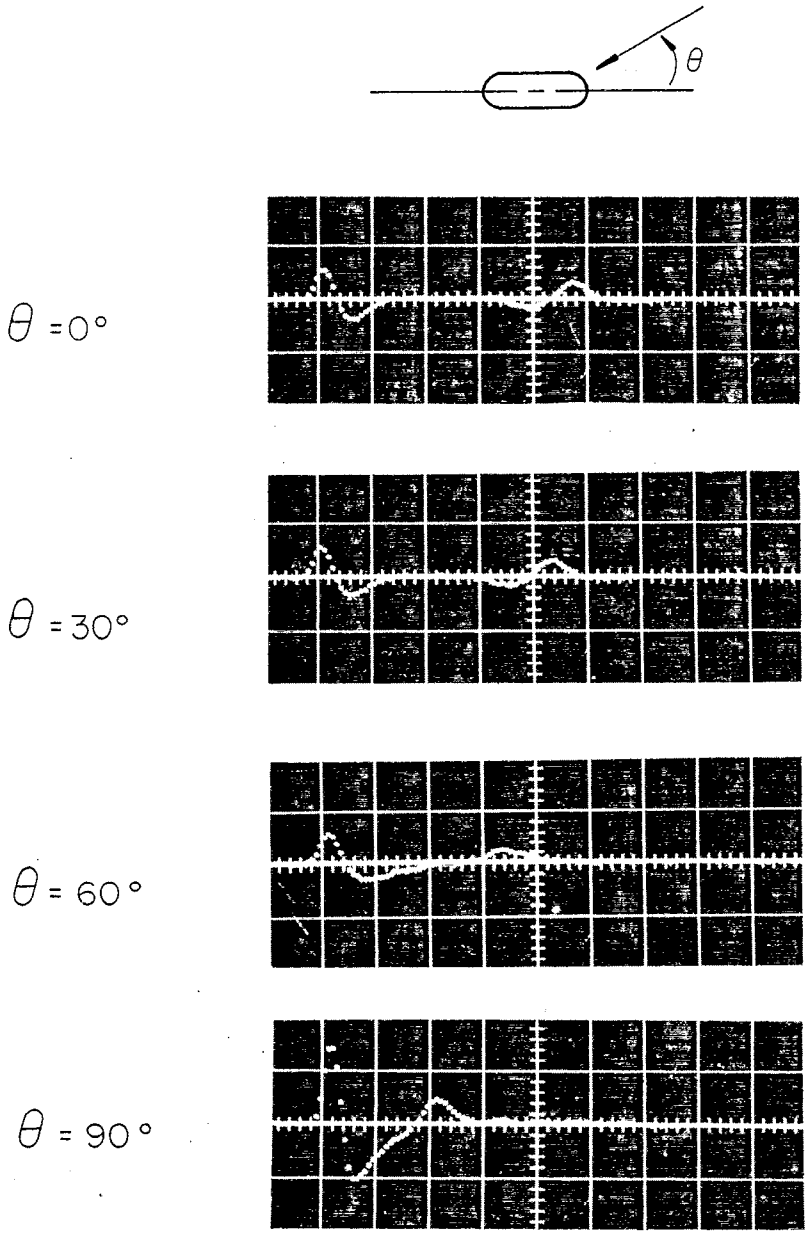

FIG. 11 Smoothed impulse response of sphere-capped cylinder (horizontal scale: 0.5 nsec/div.; vertical scale: 5 mV/div.).

traveling around the rear of the cylinder. At 30° and 60° incidence, the gradual modification from the 0° case to the 90° incidence case may be noted. At 90° incidence the shape of the response is virtually the same as it was for the right circular cylinder at 90° incidence. This is expected, since the effect of the cylinder ends appears to be negligible for this polarization and angle of incidence, as pointed out earlier.

Finally, the smoothed impulse response of a sphere-cone-sphere (with a half angle of 15°, a large sphere diameter of 8 in., and a small sphere diameter of 2 in.) is displayed in Fig. 12. For the case with axial incidence on the small sphere tip (0° incidence), Fig. 12 shows the small return from the tip, followed by a negligible return from the conical part of the structure. Next, a negative return, apparently from the joint between the large sphere and the cone, appears. This is followed by the return that can be attributed to a wave traveling around the rear spherical surface of the structure. By viewing Figs. 12 and 13 the gradual change in character of the response from the case of 0° incidence to the case of 180° incidence can be observed. For the case of axial incidence on the large sphere base (180° incidence) the initial part of the return is the same as that for the 8 in. diameter sphere shown in Fig. 10(b), as expected. This is followed by a near zero return from the conical surface, which by the way is in the geometric light shadow. Finally, the return from the tip region of the structure may be observed approximately 3.2 nsec after the initial pulse. It is also interesting to note that the initial portion of the returns for 180°, 150°, 120° and 90° incidence all possess the same shape as the initial return for the 8 in. diameter sphere shown in Fig. 10(b).

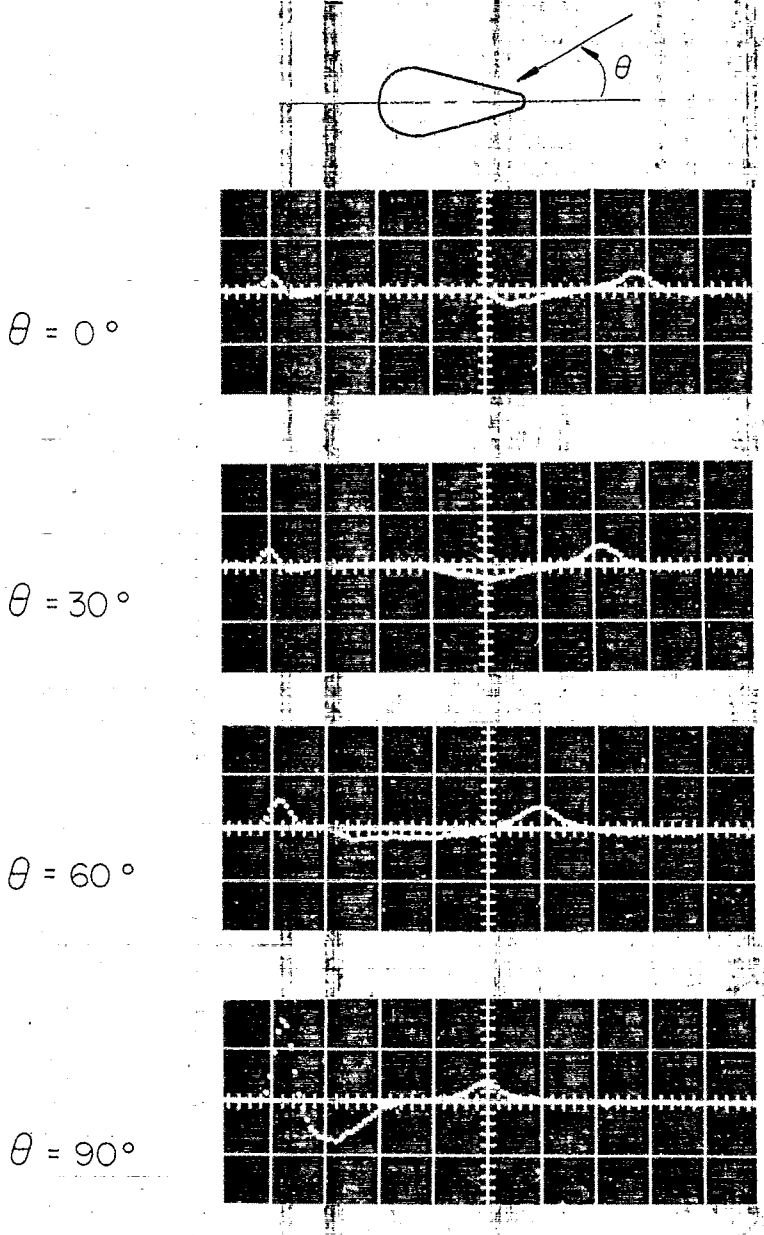

FIG. 12 Smoothed impulse response of sphere-cone-sphere (horizontal scale: 0.5 nsec/div.; vertical scale: 5 mV/div.).

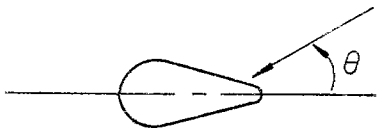

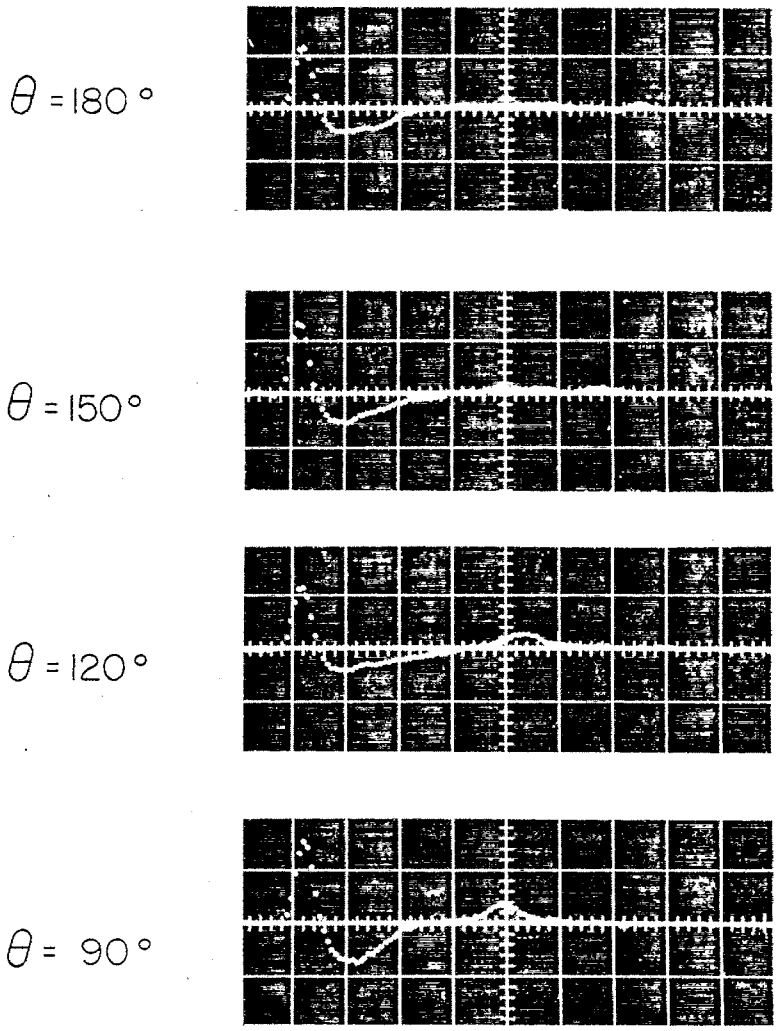

FIG. 13 Smoothed impulse response of sphere-cone-sphere (horizontal scale: 0.5 n sec/div.; vertical scale: 5 mV/div.).

SECTION 3

DISCRIMINANT ANALYZER

The basic processing philosophy employed in this study to analyze target discriminants is based on the properties of the correlation function. There are several advantages to this approach. In particular, once the appropriate data have been measured, the implementation of the processor is relatively straightforward. In addition, a correlation processor (or matched filter) maximizes the signal-to-noise ratio, and in many cases is an optimum filter. This will be discussed in more detail later.

3.1 PROCESSING PHILOSOPHY

The fundamental basis for choosing a correlation function computer for a discriminant analyzer is that the peak of the autocorrelation function is greater than any cross-correlation function under an energy normalization. This is readily understood by defining $R_{ir}(t)$ to be

$$R_{ir}(t) = \int f_i(\tau) f_r(t + \tau) d\tau$$

where $f_i(t)$ and $f_r(t)$ are two real functions and $R_{ir}(t)$ is the unnormalized cross-correlation function.

Applying the Schwarz inequality to $|R_{ir}(t)|^2$ yields

$$|R_{ir}(t)|^2 = \left|\int f_i(\tau) f_r(t + \tau) d\tau\right|^2 \leq \int |f_i(\tau)|^2 d\tau \int |f_r(\tau)|^2 d\tau$$

Dividing by $\int |f_i(\tau)|^2 d\tau$ and $\int |f_r(\tau)|^2 d\tau$ leads to

$$|\rho_{ir}(t)| = \frac{|R_{ir}(t)|}{\left[\int |f_i(\tau)|^2 d\tau\right]^{\frac{1}{2}} \left[\int |f_r(\tau)|^2 d\tau\right]^{\frac{1}{2}}}$$

Since $R_{ii}(0) = \left|\int f^2(\tau)d\tau\right|$ and $f_i(t)$ and $f_r(t)$ are real, we have

$$R_{ii}(0) = \int |f(\tau)|^2 d\tau \quad .$$

Hence,

$$|\rho_{ir}(t)| = \frac{|R_{ir}(t)|}{\left[R_{ii}(0)R_{rr}(0)\right]^{\frac{1}{2}}} \leq 1$$

or

$$|\rho_{ii}(0)| = \frac{R_{ii}(0)}{\left[R_{ii}^2(0)\right]^{\frac{1}{2}}} \leq 1 \quad .$$

Since $|\rho_{ir}(t)|$ is less than unity unless $f_i(t) \equiv kf_r(t+\tau)$ and $|\rho_{ii}(0)|$ is identically one, we see that the amount by which the maximum value of any $|\rho_{ir}(t)|$ is less than unity can be used as a measure of the ability to discriminate between the real functions $f_i(t)$ and $f_r(t)$ in the absence of noise. The smoothed or regularized impulse responses employed in this work are real functions; therefore, the above analysis can be employed.

Before passing to the discussion of the actual digital implementation of the processor, a few words regarding angular data and system noise are appropriate.[1] In particular, the number of waveforms pertaining to a particular target shape that must be stored depends on the actual shape of the target and the transmitted pulse width. It is clear that if the incident pulse is not short enough to resolve, in range, the change in location of the scattering centers as a function of angle, then a continuous angular record is not necessary. Once we accept this fact, it is clear that target response information at a number of angular orientations is all that need be stored. It is also clear

that the angular sampling spacing is related to the required number of time samples and hence to the Nyquist frequency of the system waveforms. The angular sampling frequency requirements can also be studied experimentally using the scattering range and the correlation processor. However, a detailed study of these interactions has not yet been made. The results in this report are based on angular data at a few representative angles chosen to illustrate the ideas and should not be thought of an as optimum angular sample spacing.

3.2 DIGITAL IMPLEMENTATION

In order to demonstrate and evaluate the processing philosophy presented in the previous section, the computer was programmed to implement the operations stated in the functional block diagram shown in Fig. 14. Since the scattering range data is stored digitally in the computer, the first step in the process is to compute and store the conjugate Fourier transform and energy of each reference waveform. A total of 22 waveforms were used in this study. The Fourier transform and energy of an unknown target-plus-noise waveform are also computed and stored. Once the target data are stored, we multiply the target's complex spectrum with one of the conjugate reference spectra, compute the inverse transform of the product, select the maximum value of the result and divide by the product of the target and reference energies. The maximum value of $|\rho_{ir}(t)|$ is found and $\rho_{ir}(t)$ is then stored. This process is repeated for every target in the reference library. If the target response is the k^{th} in the reference library, then the array of numbers we have stored is the k^{th} column of the correlation coefficient matrix. If we introduce targets one at a time and compute all twenty-two column vectors, then the total array, properly ordered, constitutes the correlation coefficient matrix. In the absence of noise this matrix is symmetric. The results in the noiseless case over the full system bandwidth are shown in Fig. 15. The main diagonal is unity, as expected, and the off-diagonal terms range in absolute value from 0.335 to 0.984. This array then constitutes a quantitative measure of the discriminants that exist among the target waveforms employed.

In order to obtain a measure of how the discriminants vary as a function of center frequency and bandwidth of a potential target identification system, each of the target returns was filtered and the correlation matrix was

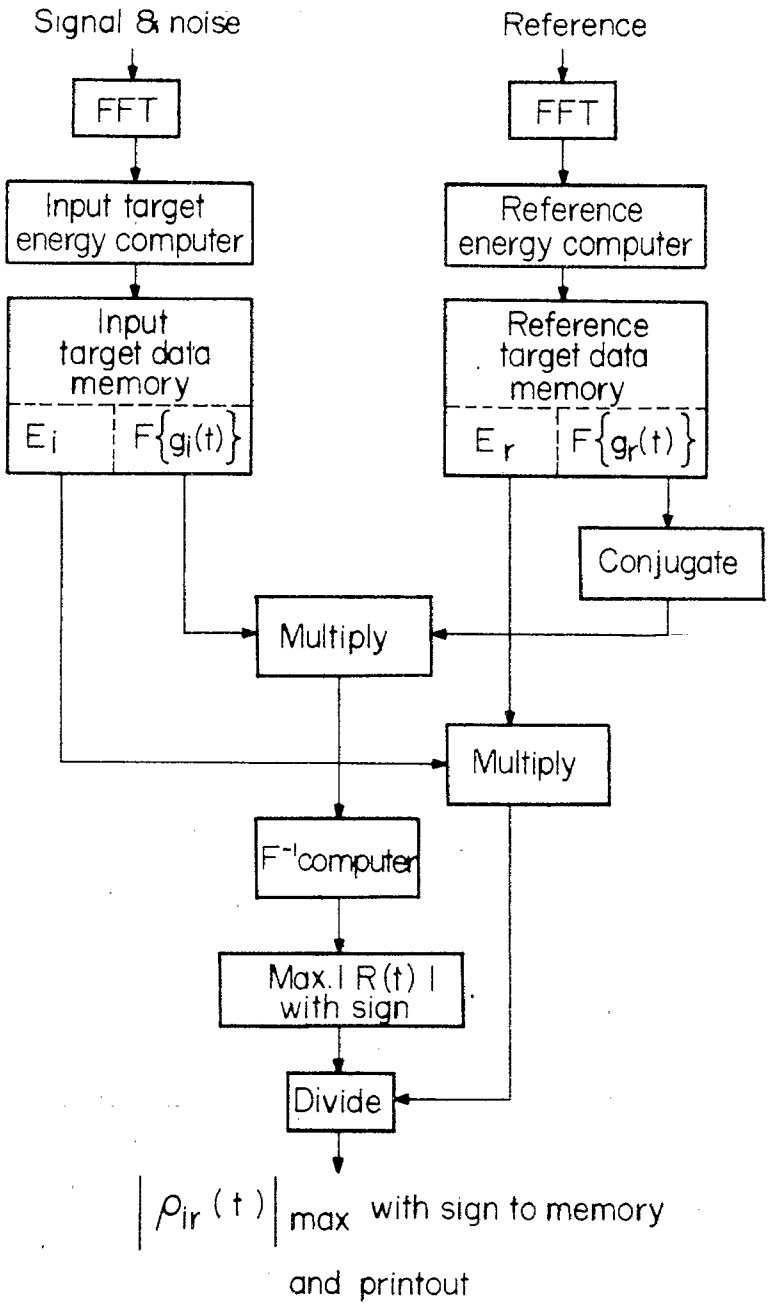

FIG. 14 Functional block diagram of the discriminant analyzer.

	CUBE		FLAT END CYLINDER				SPHERE CAPPED CYLINDER				RECTANGULAR CYLINDER				SPHERE-CONE-SPHERE							
SPHERE	0*	45*	0*	30*	60*	90*	0*	30*	60*	90*	0*	30*	60*	90*	0*	30*	60*	90*	120*	150*	180*	
1.00	.685	.811	.554	.833	.941	.723	.606	.659	.935	.736	.605	.643	.902	.639	.925	.929	.953	.961	.582	.551	.494	SPHERE
	1.00	.685	.868	.665	.678	.888	.855	.814	.688	.890	.920	.764	.783	.923	.779	.795	.761	.734	.516	.368	.392	0* CUBE
		1.00	.612	.676	.780	.608	.596	.591	.744	.619	.673	.738	.760	.532	.826	.875	.853	.811	.688	.501	-.513	45*
			1.00	.664	.571	.820	.702	.566	.595	.782	.965	.772	.595	.861	.618	.627	.570	.578	.333	.376	.484	0*
				1.00	.883	.747	.563	.570	.798	.767	.699	.578	.685	.612	.713	.748	.734	.793	.489	.443	.388	30*
					1.00	.766	.645	.665	.915	.784	.625	.701	.817	.594	.897	.913	.892	.949	.482	.471	.478	60* FLAT END CYLINDER
						1.00	.802	.792	.779	.984	.840	.779	.769	.879	.818	.808	.743	.805	-.462	-.425	.442	90*
							1.00	.836	.670	.830	.730	.855	.690	.759	.750	.756	.712	.692	.605	-.367	.370	0*
								1.00	.625	.801	.631	.677	.841	.745	.768	.769	.787	.717	.553	.374	.389	30* SPHERE CAPPED
									1.00	.806	.663	.703	.833	.678	.911	.904	.877	.943	-.431	.572	.557	60* CYLINDER
										1.00	.841	.799	.772	.845	.822	.811	.747	.826	-.460	-.448	.458	90*
											1.00	.790	.655	.866	.671	.698	.626	.651	.335	.379	.389	0*
												1.00	.656	.646	.798	.793	.727	.752	.595	.425	.442	30*
													1.00	.753	.909	.911	.947	.904	.619	.470	.480	60* RECTANGULAR CYLINDER
														1.00	.710	.696	.663	.664	-.401	.335	.404	90*
															1.00	.985	.963	.965	.637	.524	.534	0*
																1.00	.971	.969	.643	.514	.526	30*
																	1.00	.945	.714	.511	.516	60*
																		1.00	.572	.499	.516	90* SPHERE CONE SPHERE
																			1.00	.684	.621	120*
																				1.00	.749	150*
																					1.00	180*

FIG. 15 Correlation matrix of original target responses.

recomputed. The resulting matrices are shown in the appendix for various frequency-spectrum conditions. In Fig. 16 the bargraph (with expanded scale) shows the average values of the off-diagonal terms for the frequency conditions studied. The results show that the off-diagonal terms increase gradually as the cutoff frequency of the low-pass filter is reduced. When the low frequencies are removed, however, the off-diagonal terms appear, on the average, to increase more rapidly. This, of course, tends to support the contention that the major source of discriminating information is in the lower portion of the band. In addition, when the specular return was removed the average off-diagonal terms were smaller than the even unfiltered results. This is further indication (since the specular return is directly related to the optical return) that the ability to discriminate between objects of similar size on the basis of a backscattered electromagnetic field will be improved if a lower frequency (i.e., closer to the resonance region) radar is used.

Up to this point we have computed the cross-correlation functions of smoothed and filtered impulse-response waveforms of various similarly shaped targets and have used the amount by which the maximum value of any cross-correlation function is less than unity as a measure of the discriminants present in the response waveforms. In the noiseless case we can always select the greatest value in any column without error. However, the ability of the correlation technique to be a useful discriminator depends on the amount of noise immunity present. We would expect reasonably good results, not necessarily optimum, simply on the basis that the correlator or matched filter maximizes the signal-to-noise ratio. Rather than speculate further we proceed to the next section, in which optimum discriminators are theoretically investigated in various situations.

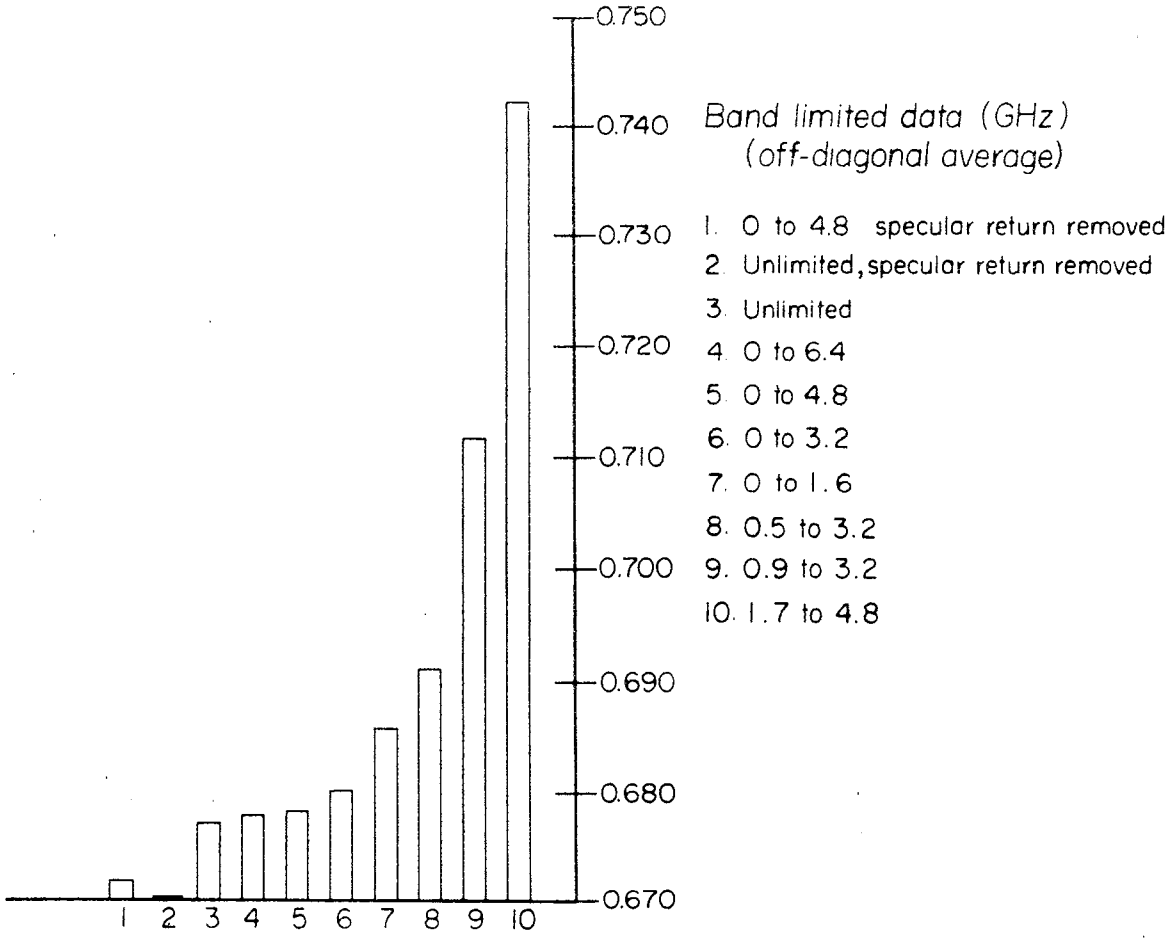

FIG. 16 Off-diagonal average of peak-limited data.

SECTION 4

THEORETICAL ANALYSIS

In this section of the report we shall review the theory of various forms of optimum discrimination.[4,5,6,7] We wish to apply this theory to the problem of identifying targets from their radar returns. Usually these returns are buried in noise. Hence, knowing the returns from targets of interest we can use the theory of optimum discrimination to identify the target that is present from its noisy radar return.

In the following discussion we shall assume that all signals and noise can be represented by a finite train of uniformly spaced time samples. The case of continuous waveforms can be handled by using the Karhunen-Loeve expansion. The results in the continuous case are analagous to the finite-sample case, where sums of samples correspond to integrals.

In Sec. 4.1 we will discuss the optimum discriminator for the case of completely known signals in additive noise of various characteristics. This case represents the ideal situation of knowing everything about the expected signal return. In Sec. 4.2 we shall consider the practical situation where the return signals have unknown parameters such as unknown amplitudes and delays.

4.1 KNOWN SIGNALS IN NOISE

In this section we shall develop the optimum discriminator in the sense of minimizing the probability of error when the signals are known exactly, but have been corrupted by additive noise. We shall assume that our observables are a finite set of uniformly spaced time samples of the pertinent waveforms. This is the form in which the actual data is known and is particularly suitable for digital operations in a computer.

Let us assume that we have a set of M signals, each of which is represented by N uniformly spaced time samples. These signals can be represented as N dimensional vectors, i.e.,

$$\underline{S}_j = \begin{bmatrix} S_{1j} \\ \vdots \\ S_{N_j} \end{bmatrix} \quad 1 \le j \le M \tag{1}$$

where

$$S_{ij} = S_j(iT) \qquad 1 \le i \le N$$

$$T = \text{sampling interval}$$

$$S_j(t) = j^{th} \text{ signal voltage .}$$

In this particular set of experiments, $M = 22$ and $N = 128$. Similarly, the additive noise is represented by the vector

$$\underline{N}_o = \begin{bmatrix} N_{o1} \\ \vdots \\ N_{oN} \end{bmatrix} \tag{2}$$

where $N_{oi} = N_o(iT)$, $1 \le i \le N$, is the discrete representation of the noise voltage $N_o(t)$.

Given the samples of a signal plus noise, we wish to decide, with a minimum probability of error, which signal is present in the noise; i.e., we

are given the vector

$$\underline{X} = \underline{S}_j + \underline{N}_o \tag{3}$$

where $\underline{S}_j$ is desired. Since an error is committed every time $\underline{S}_i$ is decided when $\underline{S}_j (i \neq j)$ is present, it follows that the total probability of error is given by

$$P_E = \sum_{\substack{i=1 \\ i \neq j}}^{M} \sum_{j=1}^{M} P\left[\underline{S}_j ; \underline{S}_i\right] \tag{4}$$

where P_E is the probability of error and $P\left[\underline{S}_j ; \underline{S}_i\right]$ is the joint probability that $\underline{S}_j$ is decided and $\underline{S}_i$ is present. We shall assume that one of the signals $\underline{S}_j$ is present in the noise; hence

$$\sum_{j=1}^{M} P\left[\underline{S}_j\right] = 1 \tag{5}$$

where $P\left[\underline{S}_j\right]$ is probability that $\underline{S}_j$ is present. From probability theory, Eq. (5) implies

$$\sum_{j=1}^{M} \sum_{i=1}^{M} P\left[\underline{S}_j ; \underline{S}_i\right] = 1 \ . \tag{6}$$

Equation (6) substituted into Eq. (4) yields

$$P_E = 1 - \sum_{j=1}^{M} P\left[\underline{S}_j ; \underline{S}_j\right] . \tag{7}$$

Equation (7) states that the total probability of making an error is equal to one minus the total probability of making correct decisions.

From the definition of conditional probability,

$$P[\underline{S}_j ; \underline{S}_i] = P[\underline{S}_j \,|\, \underline{S}_i]\, P[\underline{S}_i] \tag{8}$$

where $P[\underline{S}_j \,|\, \underline{S}_i]$ is the conditional probability that $\underline{S}_j$ is decided, given that $\underline{S}_i$ is present.

Using Eq. (8) in Eq. (7) we obtain

$$P_E = 1 - \sum_{j=1}^{M} P\left[\underline{S}_j \,|\, \underline{S}_j\right] P\left[\underline{S}_j\right] . \tag{9}$$

Hence, in order to find the total probability of error we must know the probabilities of occurrence of signals and the conditional probability of a decision. Now the a priori probabilities of occurrence of the signals have nothing to do with the noise, and we shall assume that these are known. On the other hand, the conditional probability of a decision depends upon the additive noise. In order to evaluate the conditional probabilities in Eq. (9) we must consider the decision process.

On the basis of a given vector $\underline{X}$ we must make a decision that some signal $\underline{S}_j$ is present. This means that we must partition the space of all vectors $\underline{X}$ into regions V_j, which is the decision that $\underline{S}_j$ is present. From this point of view, the conditional probability becomes

$$P[\underline{S}_j | \underline{S}_i] = P[\underline{X} \in V_j | \underline{S}_i] \tag{10}$$

where $P[\underline{X} \in V_j | \underline{S}_i]$ is the probability that $\underline{X}$ belongs to V_j, given that $\underline{S}_i$ is present. In terms of the condition probability density of the vector $\underline{X}$, given that $\underline{S}_i$ is present, Eq. (10) becomes

$$P[\underline{S}_j | \underline{S}_i] = \int_{V_j} P[\underline{X} | \underline{S}_i] \; \underline{dx} \tag{11}$$

where $P[\underline{X} | \underline{S}_i]$ is the conditional probability density of $\underline{X}$ given that $\underline{S}_i$ is present and $\underline{dx} = dx_1, dx_2, \ldots, dx_N$. The integral in Eq. (11) is over the N dimensional region V_j. Substituting Eq. (11) into Eq. (9) we obtain

$$P_E = 1 - \sum_{j=1}^{M} \int_{V_j} P[\underline{X} | \underline{S}_j] \, P[\underline{S}_j] \; \underline{dx} \; . \tag{12}$$

Since the integrands in Eq. (12) are non-negative, minimizing the total probability of error is equivalent to maximizing the sum in Eq. (12); i.e.,

$$\max \sum_{j=1}^{M} \int_{V_j} P(\underline{X} | \underline{S}_j) \, P[\underline{S}_j] \; \underline{dx} \; . \tag{13}$$

This expression is maximized by choosing the regions V_j . Consider a single vector $\underline{X}$. This single vector can contribute to only one integrand in expression (13), since each vector $\underline{X}$ can belong to one and only one region V_j . The strategy then is to place $\underline{X}$ in a region V_{j_o} so as to maximize its contribution to expression (13). Since the integrand is non-negative, this maximum contributor occurs when $\underline{X}$ is placed in the region V_{j_o} , where j_o maximizes the expression

$$P(\underline{X}|\underline{S}_j)\ P[\underline{S}_j] \ . \tag{14}$$

The region V_{j_o} is simply the set of all $\underline{X}$'s which satisfy the expression

$$P(\underline{X}|\underline{S}_{j_o})\ P[\underline{S}_{j_o}] > P(\underline{X}|\underline{S}_j)\ P[\underline{S}_j] \quad \text{all} \quad j \neq j_o \ . \tag{15}$$

Hence, the decision rule is: decide $\underline{S}_{j_o}$ if j_o maximizes $P(\underline{X}|\underline{S}_j)\ P[\underline{S}_j]$ for the given $\underline{X}$. If, for the particular value of $\underline{X}$ two or more values of j maximize expression (14), then it does not matter which of these values is chosen, since the choice will not affect the probability of error.

A block diagram of the optimum discriminator is shown in Fig. 17. This discriminator calculates the probability $P(\underline{X}|\underline{S}_j)\ P[\underline{S}_j]$ and selects the one that has the greatest output. In the following sections we shall find the forms that this discriminator takes when particular forms of noise are present.

4.1.1 Uniform Independent Noise

In this section we determine the form of the discriminator when the additive noise is uniform and independent with zero mean and range R. A block diagram of the discriminator appears in Fig. 18.

Consider a single sample of the vector $\underline{X}$, i.e., X_k . This component (Eq. (3)) is the sum of a constant and uniform random variable. Hence,

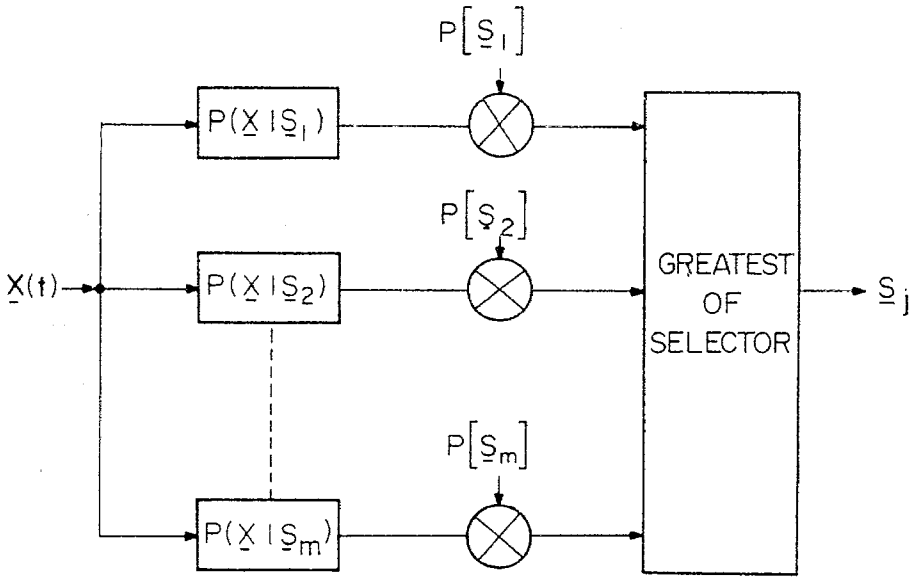

FIG. 17 Minimum probability discriminator using probability computers.

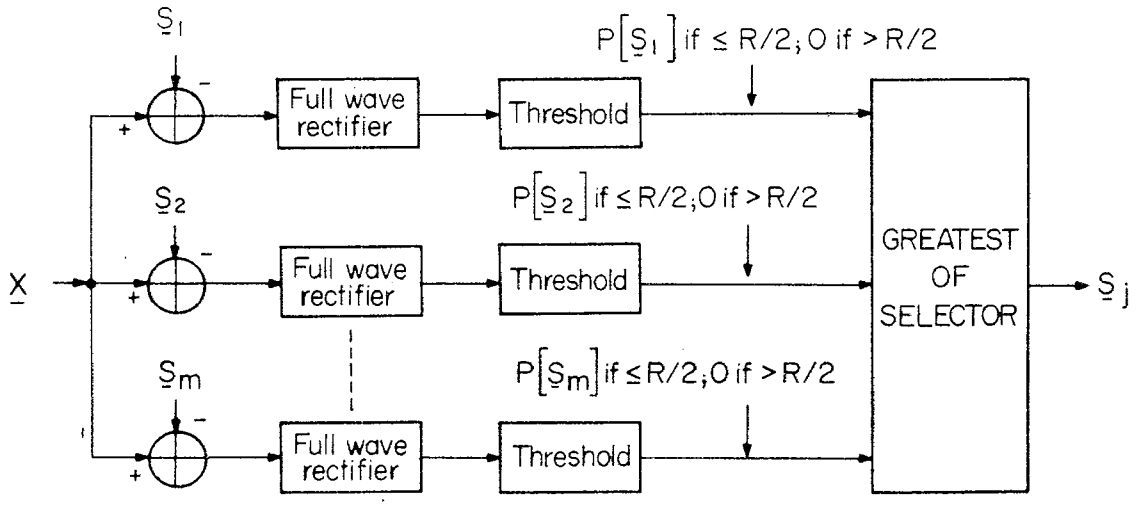

FIG. 18 Minimum probability discriminator for uniform noise.

$\underline{X}_k$ is a uniform random variable with mean equal to the constant S_{kj}. Thus, the conditional density of this component, given that $\underline{S}_j$ is present, is

$$P(\underline{X}_k|\underline{S}_j) = \frac{1}{R} \qquad |X_k - S_{kj}| \leq \frac{R}{2}$$
$$= 0 \qquad \text{elsewhere} . \tag{16}$$

Since the noise is independent, the resulting joint density for the vector $\underline{X}$ is simply the product of the densities of the components, i.e.,

$$P(\underline{X}|\underline{S}_j) = \prod_{k=1}^{N} P(\underline{X}_k|\underline{S}_j) . \tag{17}$$

From Eq. (17) we find that the decision rule in this case is: choose $\underline{S}_{j_o}$ if j_o maximizes

$$\left\{ \prod_{k=1}^{N} p(X_k|\underline{S}_j) \right\} P[\underline{S}_j] . \tag{18}$$

Using Eq. (16) we find that the decision rule becomes: choose $\underline{S}_{j_o}$ if

$$|X_k - S_{kj_o}| \leq \frac{R}{2} \qquad 1 \leq k \leq N . \tag{19}$$

If more than one value of j satisfies Eq. (19), then choose the value of j which has the greatest a priori probability $P[\underline{S}_j]$. A consideration of the

above process will show that at least one value of j will satisfy Eq. (19).

Let us calculate the total probability of error for this case. Using Eq. (17) in Eq. (11) we obtain

$$P_E = 1 - \sum_{j=1}^{M} \int_{V_j} \left\{ \prod_{k=1}^{N} P(X_k | \underline{S}_j) \right\} P[\underline{S}_j] \ \underline{dx} \tag{20}$$

where V_j is determined by Eq. (19). Upon considering Eqs. (16), (19) and (20), we find that the probability of error becomes

$$P_E = \sum_{i=2}^{M} \sum_{j=1}^{i-1} \left\{ \prod_{k=1}^{N} U\left(1 - \frac{|S_{kj} - S_{ki}|}{R}\right) \right\} \min \{P[S_j], P[S_i]\} \tag{21}$$

where

$$\begin{aligned} U(x) &= x \qquad x > 0 \\ &= 0 \qquad x \leq 0 \\ \min\{a,b\} &= a \qquad a \leq b \\ &= b \qquad a > b \ . \end{aligned}$$

4.1.2 Gaussian Independent Noise

In this section we shall determine the form of the discriminator when we have additive white Gaussian noise with zero mean and variance σ^2.

Consider a single component of the vector $\underline{X}$, i.e., X_k. From Eq. (3) we see that this component is the sum of a constant S_{kj} and Gaussian random variable with zero mean. Hence, the sum will be a Gaussian random variable with mean S_{kj}. The conditional density of X_k, given that $\underline{S}_j$ is

$$\sigma^2 \ln P[\underline{S}_j] + \sum_{k=1}^{N} X(kT)\, S_j(kT) - \frac{1}{2} E_j \qquad (28)$$

where

$$E_j = \sum_{k=1}^{N} S_j^2\,(kT) \ .$$

Hence, the optimum discriminator computes the discrete cross-correlation between $X(t)$ and $S_j(t)$ at $t = 0$. The form of this discriminator is depicted in Fig. 19. We note that the cross correlations can also be represented as matched-filter outputs evaluated at $t = NT$.

Let us calculate the total probability of error for this discriminator. The total probability of error (Eq. (12)) requires calculation of the integral

$$P[\underline{S}_i | \underline{S}_i] = \int_{V_i} P(\underline{X}|\underline{S}_i) \ \underline{dx} \qquad (29)$$

where V_i is the set of vectors $\underline{X}$ for which i maximizes expression (27). Let us define a new vector $\underline{z}$:

$$\underline{z} = \begin{bmatrix} z_1 \\ \vdots \\ z_M \end{bmatrix} \qquad (30)$$

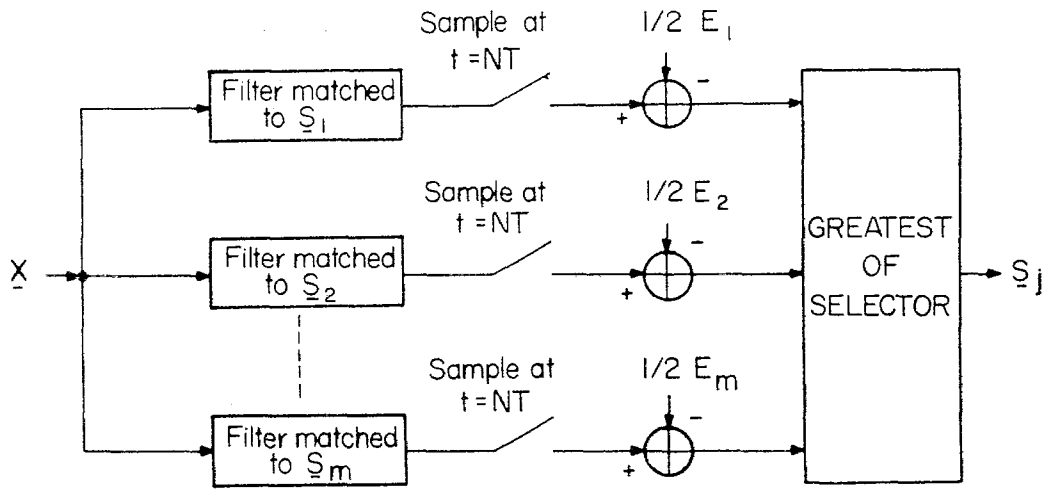

FIG. 19 Minimum probability discriminator for Gaussian noise.

present, will be

$$P(X_k|\underline{S}_j) = [2\pi\sigma^2]^{-\frac{1}{2}} \exp\left\{-\frac{(X_k - S_{kj})^2}{2\sigma^2}\right\} \tag{22}$$

where

σ^2 = variance of the noise.

Since the noise is independent, the resulting density for the entire vector $\underline{X}$ will simply be the product of the densities of the individual components; i.e.,

$$P(\underline{X}|\underline{S}_j) = \prod_{k=1}^{N} P(X_k|\underline{S}_j) \tag{23}$$

or

$$P(\underline{X}|\underline{S}_j) = [2\pi\sigma^2]^{-N/2} \exp\left\{-\frac{1}{2\sigma^2}\sum_{k=1}^{N}(X_k - S_{kj})^2\right\} . \tag{24}$$

Substituting Eq. (24) into the decision rule, we find that it becomes: choose $\underline{S}_{j_o}$ if j_o maximizes

$$P[\underline{S}_j]\,[2\pi\sigma^2]^{-N/2} \exp\left\{-\frac{1}{2\sigma^2}\sum_{k=1}^{N}(x_k - S_{kj})^2\right\} . \tag{25}$$

Maximizing expression (25) is equivalent to maximizing

$$\ln P[\underline{S}_j] - \frac{1}{2\sigma^2} \sum_{k=1}^{N} (X_k - S_{kj})^2 \tag{26}$$

since the natural logarithmic function is monotonically increasing. Expression (26) can be further reduced by eliminating additive terms which are independent of j and thus will not affect the maximization. Hence, the decision rule becomes: choose $\underline{S}_{j_o}$ if j_o maximizes

$$\sigma^2 \ln P[\underline{S}_j] + \sum_{k=1}^{N} X_k S_{kj} - \frac{1}{2} E_j \tag{27}$$

where

$$E_j = \sum_{k=1}^{N} S_{kj}^2 = \text{energy in } \underline{S}_j \ .$$

In the equally likely case that the $P[\underline{S}_j]$ become independent of j, they can be eliminated from expressions (26) and (27) without affecting the maximization. In this case, expression (26) can be interpreted as describing a discriminator which selects the signal that is closest in mean-square-error sense to the observed vector $\underline{X}$.

Referring to Eqs. (1) and (2), we see that Eq. (27) can be expressed in the form

where

$$z_i = \underline{S}_i^T \underline{X} + \ln P[\underline{S}_i] - \frac{1}{2} E_i \quad . \tag{31}$$

The vector $\underline{z}$ can also be expressed in terms of a single matrix equation

$$\underline{z} = \underline{\underline{S}}^T \underline{X} + \ln \underline{P} - \frac{1}{2} \underline{E} \tag{32}$$

where

$$\underline{\underline{S}} = \left[\underline{S}_1 \vdots \underline{S}_2 \vdots \cdots \vdots \underline{S}_M \right]$$

$$\ln \underline{P} = \begin{bmatrix} \ln P[\underline{S}_1] \\ \vdots \\ \ln P[\underline{S}_M] \end{bmatrix}$$

$$\underline{E} = \begin{bmatrix} E_1 \\ \vdots \\ E_M \end{bmatrix} \quad .$$

In terms of the vector $\underline{z}$ the region V_i is just the set of $\underline{z}$ which satisfy

$$z_i > z_j \qquad \text{for all } j \neq i \quad . \tag{33}$$

The desired probability in Eq. (29) thus becomes the probability that (33) is satisfied, given that $\underline{S}_i$ is present; i.e.

$$P[\underline{S}_i|\underline{S}_i] = \int_{-\infty}^{+\infty} dz_i \int_{-\infty}^{z_i} dz_1 \cdots \int_{-\infty}^{z_i} dz_M \, [P(\underline{z}|\underline{S}_i)] \qquad (34)$$

Now since $\underline{z}$ is a linear transformation of the Gaussian random vector $\underline{x}$, $\underline{z}$ will be a Gaussian random vector with a conditional density of[8]

$$P(\underline{z}|\underline{S}_i) = [2\pi|\underline{\underline{\Phi}}|]^{-N/2} \exp\{-\tfrac{1}{2}(\underline{z}-\underline{M})^T \underline{\underline{\Phi}}^{-1} (\underline{z}-\underline{M})\} \qquad (35)$$

where

$$\underline{\underline{\Phi}} = \sigma^2 \underline{\underline{S}}^T \underline{\underline{S}}$$

$$\underline{M} = \underline{\underline{S}}^T \underline{S}_i + \ln \underline{P} - \tfrac{1}{2} \underline{E} \quad .$$

Such an expression substituted into Eq. (34) is extemely difficult to evaluate directly. Therefore it may be more practical to find the total probability of error through Monte Carlo techniques.

4.1.3 Correlated Gaussian Noise

In this section we shall investigate the case of discriminating signals in additive correlated Gaussian noise with zero mean. We shall show that this case can be solved simply by prewhitening the noise and by using the discriminator derived in Sec. 4.1.2.

Consider the random vector $\underline{X}$ when $\underline{S}_j$ is present. From Eq. (3)

we see that the vector $\underline{X}$ will be a jointly Gaussian random variable with mean equal to $\underline{S}_j$;[8] i.e.,

$$p(\underline{X}|\underline{S}_j) = [2\pi|\underline{\underline{\Phi}}|]^{-N/2} \exp\{-\frac{1}{2}(\underline{X}-\underline{S}_j)^T \underline{\underline{\Phi}}^{-1} (\underline{X}-\underline{S}_j)\} \tag{36}$$

where

$$\underline{\underline{\Phi}} = [\Phi_{ij}] = \text{covariance matrix of noise}$$

$$\Phi_{ij} = E[N_{oi}N_{oj}] .$$

Substituting Eq. (36) into the decision rule, it becomes: choose $\underline{S}_{j_o}$ where j_o maximizes

$$P[\underline{S}_i][2\pi|\underline{\underline{\Phi}}|]^{-N/2} \exp\{-\frac{1}{2}(\underline{X}-\underline{S}_j)^T \underline{\underline{\Phi}}^{-1} (\underline{X}-\underline{S}_j)\} . \tag{37}$$

Maximizing expression (37) is equivalent to maximizing

$$\ln P[\underline{S}_i] + \underline{X}^T \underline{\underline{\Phi}}^{-1} \underline{S}_j - \frac{1}{2} \underline{S}_j \underline{\underline{\Phi}}^{-1} \underline{S}_j \tag{38}$$

since the natural logarithmic function is monotonically increasing. Let the inverse covariance matrix be expressed as a product of a matrix and its transpose:

$$\underline{\underline{\Phi}}^{-1} = \underline{\underline{A}}^T \underline{\underline{A}} \tag{39}$$

where $\underline{\underline{A}}$ is a triangular nonsingular matrix. This is possible, since $\underline{\underline{\Phi}}$ is positive definite. Now let us define a vector $\underline{Y}$ and set of vectors $\underline{S}'_j$ such that

$$\underline{Y} = \underline{\underline{A}}\underline{X} \tag{40}$$

$$\underline{S}'_j = \underline{\underline{A}}\underline{S}_j \quad 1 \leq j \leq M \quad . \tag{41}$$

Then expression (38) becomes

$$\ln P[\underline{S}_i] + \underline{Y}^T \underline{S}'_j - \frac{1}{2} \underline{S}'^T_j \underline{S}'_j \quad . \tag{42}$$

We note that the decision rule is now the same as the decision rule in Sec. 4.1.2 except that the vector $\underline{Y}$ replaces the vector $\underline{X}$ and the signal vectors $\underline{S}'_j$ replace $\underline{S}_j$. Therefore, if we use $\underline{Y}$ as an input to the discriminator of Sec. 4.1.2 with the vectors $\underline{S}'_j$ replacing the vectors $\underline{S}_j$, the resulting discriminator will be optimum. Equation (40) represents a linear filter operating on the vector $\underline{X}$. The effect of this filter on the signals is given by Eq. (41). The effect on the noise is given by Gaussian noise of covariance[8]

$$\underline{\underline{\Phi}}' = \underline{\underline{A}}\,\underline{\underline{\Phi}}\,\underline{\underline{A}}^T \tag{43}$$

where $\underline{\underline{\Phi}}'$ is the covariance matrix of the output noise. Now Eq. (39) substituted into Eq. (43) yields

$$\underline{\underline{\Phi}}' = (\underline{\underline{A}}^T\underline{\underline{A}})^{-1}\,\underline{\underline{A}}^T = \underline{\underline{A}}\underline{\underline{A}}^{-1}(\underline{\underline{A}}^{-1}\underline{\underline{A}})^T = \underline{\underline{I}} \tag{44}$$

where $\underline{\underline{I}}$ is the identity matrix. Hence, the resulting output is white (uncorrelated).

4.2 SIGNALS WITH UNKNOWN PARAMETERS

In this section we shall consider an optimum discriminator when the observed signal in noise has unknown parameters. In particular, we shall be interested in signals with unknown amplitudes: i.e., signals of the form $af(t)$ where a is unknown. We will also be interested in signals with unknown delays and signals with both unknown amplitude and delay.

We recall from Sec. 4.1 that we need the conditional density $P(\underline{X}|\underline{S}_j)$ in order to discriminate with minimum probability of error. Now suppose that the observed signals in noise depend upon a parameter α ; i.e., the vector $\underline{X}$ is of the form

$$\underline{X} = \underline{S}_{j,\alpha} + \underline{N}_0 \tag{45}$$

where

$$\underline{S}_{j,\alpha} = \begin{bmatrix} S_{1j,\alpha} \\ \vdots \\ S_{Nj,\alpha} \end{bmatrix} .$$

If the parameter α is independent of the noise and the original unperturbed signals, then the desired conditional density will be

$$P(\underline{X}|\underline{S}_j) = \int P(\underline{X}|\underline{S}_{j,\alpha}) \, P(\alpha) \, d\alpha \tag{46}$$

where $P(\underline{X}|\underline{S}_{j,\alpha})$ = conditional probability density of $\underline{X}$ given $\underline{S}_{j,\alpha}$

$P(\alpha)$ = probability density of α .

In many cases either the integral in Eq. (46) is difficult to implement or $P(\alpha)$ is unknown. In this case we would like to find a discriminator that approximates using Eq. (46) in some sense. Suppose that we desired to find the correct signal together with the correct parameter. Then from Sec. 4.1 we should select the α_0 and the j_0 which maximize

$$P(\underline{X}|\underline{S}_{j,\alpha}) \; P(\alpha) \; P[\underline{S}_j] \; . \tag{47}$$

If we ignore the value of α and simply decide that $\underline{S}_{j_0}$ is present, our decision rule becomes: choose $\underline{S}_{j_0}$ if j_0 maximizes

$$\max_{\alpha} \{P(\underline{X}|\underline{S}_{j,\alpha}) \; P(\alpha)\} \; P[\underline{S}_j] \; . \tag{48}$$

Clearly, this rule is not optimum because it assumes a penalty for confusing the α's for the same $\underline{S}_j$, whereas the correct rule would assign no penalty for this mistake. For the rest of the discussion we shall assume that all signals are equally likely and all parameter values are equally likely. Under this assumption, the decision rule becomes: choose $\underline{S}_{j_0}$ if j_0 maximizes

$$\max_{\alpha} \{P(\underline{X}|\underline{S}_{j,\alpha})\} \; . \tag{49}$$

The discriminator determined by expression (49) chooses the $\underline{S}_j$ that has most likely produced the observed vector $\underline{X}$. Hence, this discriminator is optimum in the maximum likelihood sense.

4.2.1 Signals with Unknown Amplitudes

In this section we shall find the maximum likelihood discriminator for signals with unknown amplitudes in Gaussian uncorrelated noise. The more general case of correlated Gaussian noise can be handled by first prewhitening the noise (see Sec. 4.1.3).

Assume that the observed vector $\underline{X}$ is of the form

$$\underline{X} = m\underline{S}_j + \underline{N}_o \qquad 1 \leq j \leq M \tag{50}$$

where m is the unknown amplitude of the signal. Then the resulting conditional density for $\underline{X}$, given $\underline{S}_{j,m}$, will be

$$P(\underline{X}|\underline{S}_{j,m}) = [2\pi\sigma^2]^{-N/2} \exp\left\{-\frac{1}{2\sigma^2}\sum_{k=1}^{N}(X_k - mS_{kj})^2\right\} . \tag{51}$$

The density $P(\underline{X}|\underline{S}_{j,m})$ will be maximized if and only if the sum of Eq. (51) is minimized. Therefore, we must find the minimum of

$$\sum_{k=1}^{N}(X_k - mS_{kj})^2 = \sum_{k=1}^{N}X_k^2 - 2m\sum_{k=1}^{N}X_kS_{kj} + m^2\sum_{k=1}^{M}S_{kj}^2 . \tag{52}$$

With a little algebraic manipulation Eq. (52) becomes

$$\sum_{k=1}^{N} (X_k - mS_{kj})^2 = E_j \left\{ m - \frac{\sum_{k=1}^{N} X_k S_{kj}}{E_j} \right\}^2 + \sum_{k=1}^{N} X_k^2 - \frac{\left(\sum_{k=1}^{N} X_k S_{kj} \right)^2}{E_j} \quad . \tag{53}$$

The minimum of the sum from Eq. (53) for arbitrary m is

$$\min_m \left\{ \sum_{k=1}^{N} (X_k - mS_{kj})^2 \right\} = \sum_{k=1}^{N} X_k^2 - \frac{\left(\sum_{k=1}^{N} X_k S_{kj} \right)^2}{E_j} \quad . \tag{54}$$

The required density for the decision rule is then

$$\max_m P(\underline{X} | S_{j,m}) = \left[2\pi\sigma^2 \right]^{-N/2} \exp \left\{ -\frac{1}{2\sigma^2} \left(\sum_{k=1}^{N} X_k^2 - \frac{1}{E_j} \left[\sum_{k=1}^{N} X_k S_{kj} \right]^2 \right) \right\} . \tag{55}$$

In the decision rule we must maximize Eq. (55) with respect to j . Since the exponential function is monotonically increasing, this is equivalent to maximizing

$$- \sum_{k=1}^{N} X_k^2 + \frac{1}{E_j} \left(\sum_{k=1}^{N} X_k S_{kj} \right)^2 . \tag{56}$$

Expression (56) can be further simplified, since maximizing expression (56) is equivalent to maximizing

$$\frac{\left| \sum_{k=1}^{N} X_k S_{kj} \right|}{\sqrt{E_j}} \quad . \tag{57}$$

The resulting decision rule is: choose $\underline{S}_{j_o}$ if j_o maximizes expression (57).

This decision rule should be compared to the decision rule we obtained in Sec. 4.1.2 for known signals. There are two significant differences. One is that we use the magnitude of the cross-correlation itself. Secondly, we divide by the energy instead of subtracting it. The form of this discriminator is depicted in Fig. 20.

Let us also find the decision rule when the amplitude parameter m is restricted to positive values. This would apply in systems where the polarity of the signals is known, as, for example, in scattering problems. We must maximize the conditional density in Eq. (51) under the restriction of positive m. This is equivalent to maximizing Eq. (53) for positive m, which yields

$$\max_{m>0} \sum_{k=1}^{N} (X_k - mS_{kj})^2 = \sum_{k=1}^{N} X_k^2 - \frac{1}{E_j} \left\{ \max \left[0, \sum_{k=1}^{N} X_k S_{kj} \right] \right\} \tag{58}$$

where

$$\max [0,a] = a \qquad a > 0$$
$$= 0 \qquad a \leq 0 \quad .$$

Substituting Eq. (58) into the decision rule and passing through the same equivalences that we used previously, we find that the resulting decision rule is: choose S_{j_o} if j_o maximizes

$$\max \left[0, \frac{1}{\sqrt{E_j}} \sum_{k=1}^{N} N_k S_{kj} \right] . \qquad (59)$$

The form of this discriminator is shown in Fig. 21.

4.2.2 Signals with Unknown Delays

In this section we shall find the maximum likelihood discriminator for known signals with unknown delays in Gaussian uncorrelated noise. Again, we may handle the more general case of correlated Gaussian noise by first pre-whitening the noise.

Assume that the observed vector $\underline{X}$ is of the form

$$X = S_{j,\tau} + N_o \qquad 1 \le j \le M \qquad (60)$$

where

$$S_{kj,\tau} = S_j(kT-\tau)$$

$$\tau = \text{delay} \quad .$$

Usually the function $S_j(t)$ is known only at uniformly spaced points in time. Therefore, it will be necessary to approximate Eq. (60) by

$$\underline{X} = \underline{S}_{j,\ell} + \underline{N}_o \qquad 1 \le j \le M \qquad (61)$$

where

$$S_{jk,\ell} = S_j(kT-\ell T)$$

$$\ell = \text{unknown integer} \quad .$$

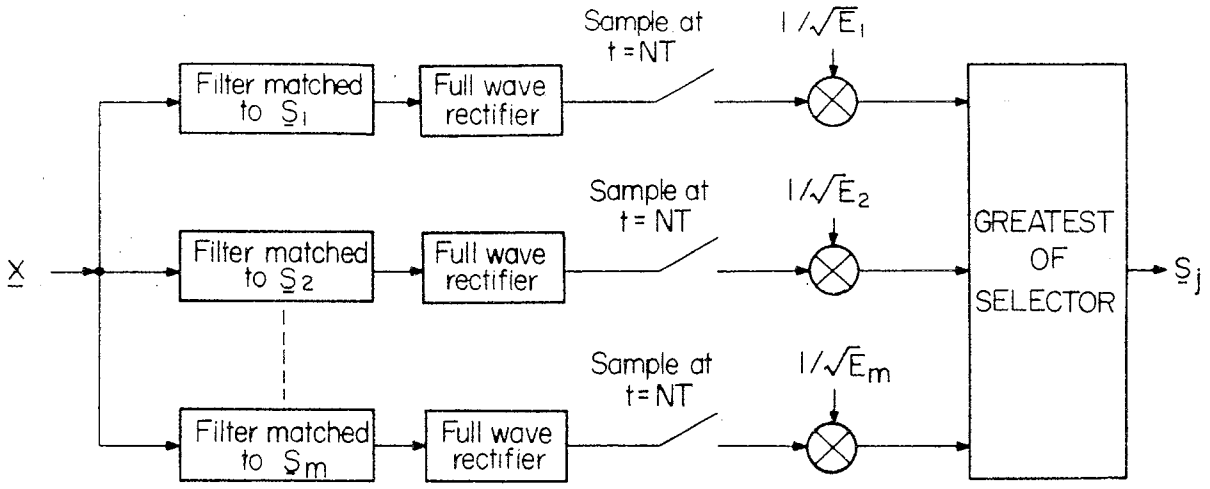

FIG. 20 Likelihood discriminator for arbitrary signal amplitude.

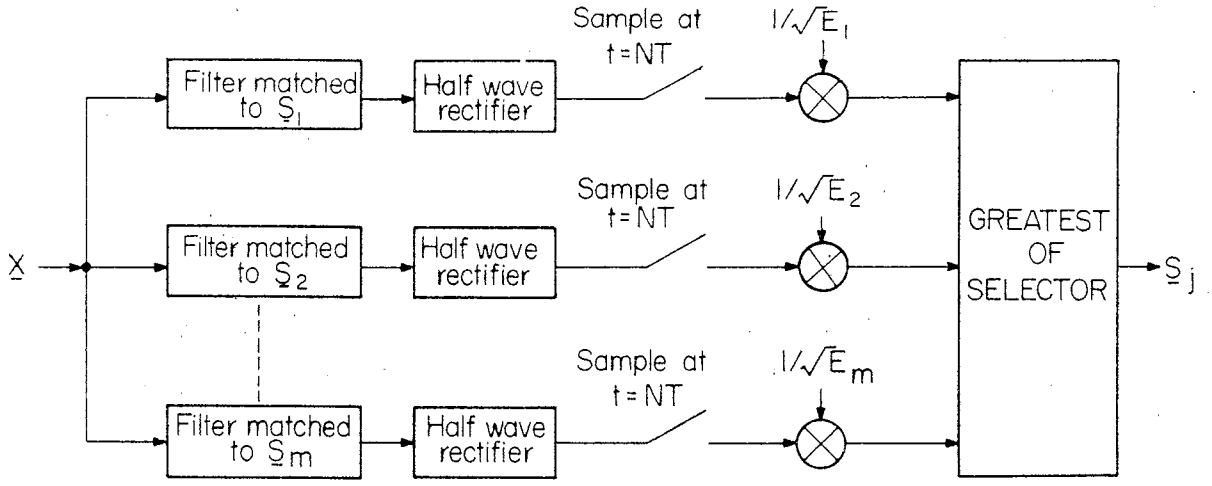

FIG. 21 Likelihood discriminator for arbitrary positive signal amplitude.

This approximation should be good if the sampling interval T is sufficiently small. The conditional probability density of $\underline{X}$, given $\underline{S}_{j,\ell}$, will be

$$P(\underline{X}|\underline{S}_{j,\ell}) = [2\pi\sigma^2]^{-N/2} \exp\left\{-\frac{1}{2\sigma^2}\sum_{k=1}^{N}(X_k - S_{k,j,\ell})^2\right\} . \qquad (62)$$

Using the same methods that were used in previous sections, we find that the decision rule is: choose $\underline{S}_{j_o}$ if j_o maximizes

$$\max_{\ell}\left\{\sum_{k=1}^{N} X_k S_{ki,\ell} - \frac{1}{2}\sum_{k=1}^{N} S_{ki,\ell}^2\right\} . \qquad (63)$$

Assume that N is sufficiently large so that

$$\sum_{k=1}^{N} S_{kj,\ell}^2 = \sum_{k=1}^{N} S_j\left((k-\ell)T\right)^2 = \sum_{k=1}^{N} S_{kj}^2 = E_j . \qquad (64)$$

This will be possible if $S_j(t)$ can be represented by a finite train of uniformly spaced samples. In this case the decision rule is: choose $\underline{S}_{j_o}$ if j_o maximizes

$$\max_{\ell}\sum_{k=1}^{N} X_k S_{kj,\ell} - \frac{1}{2}E_j . \qquad (65)$$

Now expression (65) can be expressed in terms of the original time functions, becoming

$$\max_{\ell} \sum_{k=1}^{N} X(kT)\, S_j\left((k-\ell)T\right) - \tfrac{1}{2}E_j \quad . \tag{66}$$

Thus, we see that this decision rule calculates the peak of the discrete correlation function between $X(\ell)$ and $S_j(t)$ (see Fig. 22). This compares to the discriminator for known signals (Sec. 4.1.2), which uses the cross-correlation at $t=0$.

4.2.3 Signals with Unknown Amplitudes and Delays

In this section we shall find the maximum likelihood discriminator for signals with unknown amplitudes and delays in Gaussian uncorrelated noise. Gaussian correlated noise may be handled by prewhitening the noise.

Assume that the observed vector $\underline{X}$ is of the form

$$\underline{X} = m\underline{S}_{j,\ell} + \underline{N}_o$$

where

$$S_{kj,\ell} = S_j(kT - \ell T) \quad .$$

Hence, the conditional probability density of $\underline{X}$, given $\underline{S}_{j,\ell,m}$, will be

$$P(\underline{X}|\underline{S}_{j,\ell,m}) = \left[\, 2\pi\sigma^2 \,\right]^{-N/2} \exp\left\{ -\frac{1}{2\sigma^2} \sum_{k=1}^{N} (X_k - mS_{kj,\ell})^2 \right\} . \tag{68}$$

In terms of the conditional density, the decision rule is: choose $\underline{S}_{j_o}$ if j_o maximizes

$$\max_{\ell} \max_{m} p(\underline{X}|\underline{S}_{j,\ell,m}) \quad . \tag{69}$$

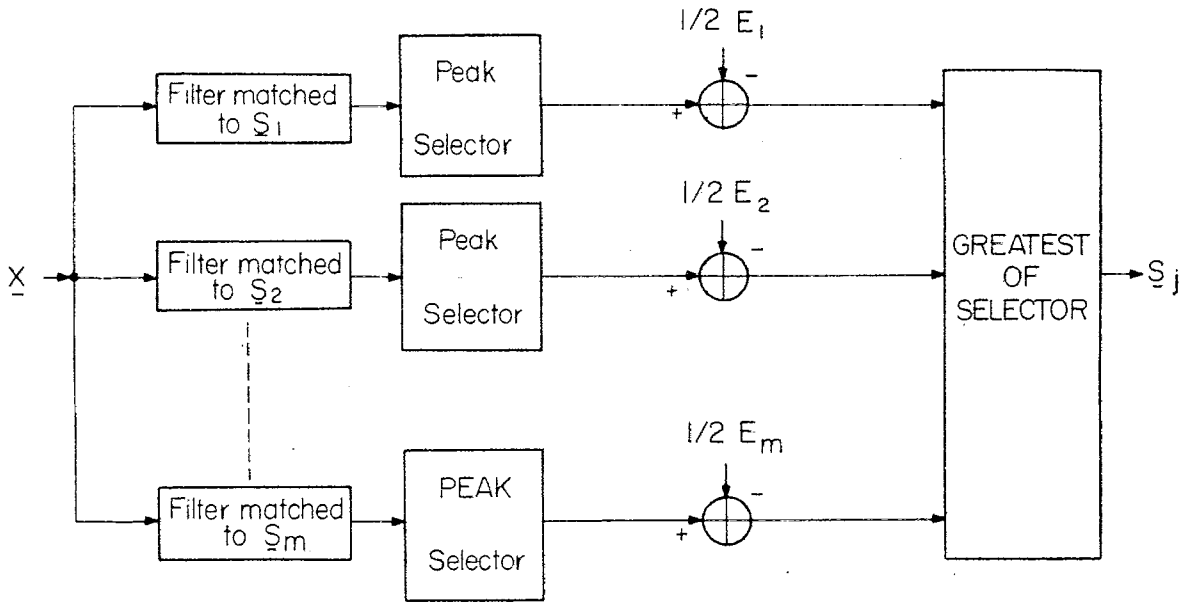

FIG. 22 Likelihood discriminator for arbitrary signal delay.

From Sec. 4.2.1 we can perform the maximization with respect to m . Hence, the decision rule becomes: choose $\underline{S}_{j_o}$ if j_o maximizes

$$\max_{\ell} \left\{ \frac{\left| \sum_{k=1}^{N} X_k S_{kj,\ell} \right|}{\sqrt{E_j}} \right\} . \tag{70}$$

where Eq. (64) is valid. In this rule we must compute the peak magnitude of the cross-correlation function between $X(t)$ and $S_j(t)$ (see Fig. 23).

Similarly, we find the decision rule for the case of positive m to be: choose $\underline{S}_{j_o}$ if j_o maximizes

$$\max_{\ell} \left\{ \max \left[0, \frac{1}{\sqrt{E_j}} \sum_{k=1}^{N} X_k S_{kj,\ell} \right] \right\} . \tag{71}$$

The form of this discriminator is shown in Fig. 24.

A discussion of the results of digital simulation of many of the ideas presented in the preceding paragraphs is contained in Sec. 5.

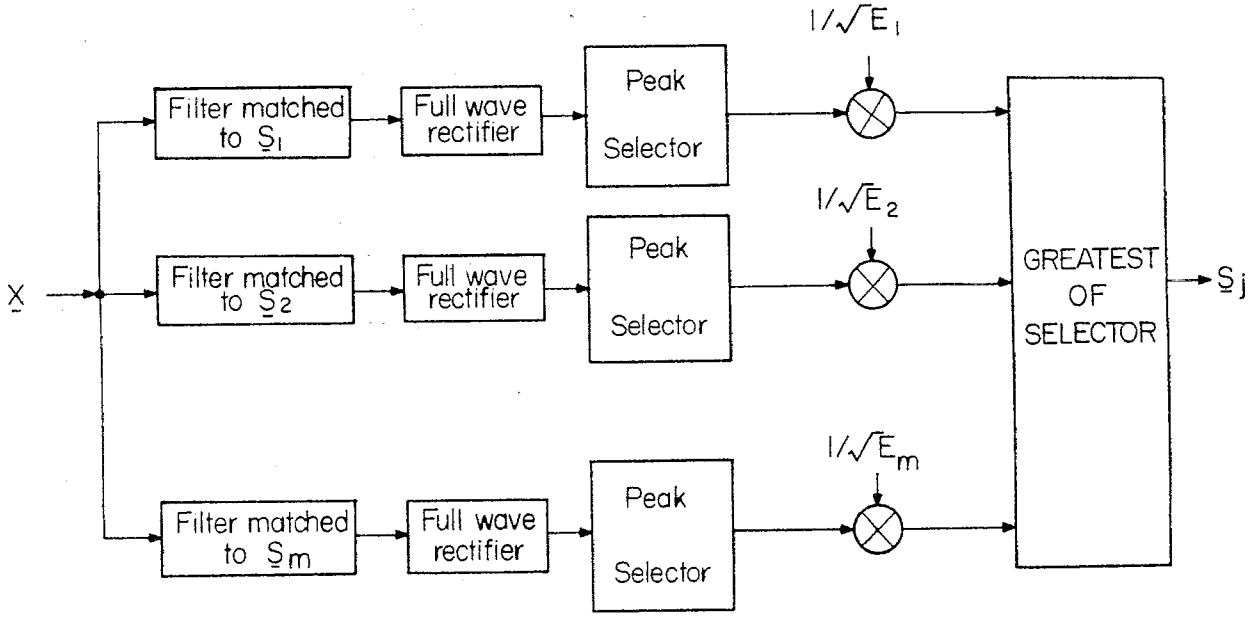

FIG. 23 Likelihood discriminator for arbitrary signal amplitude and delay.

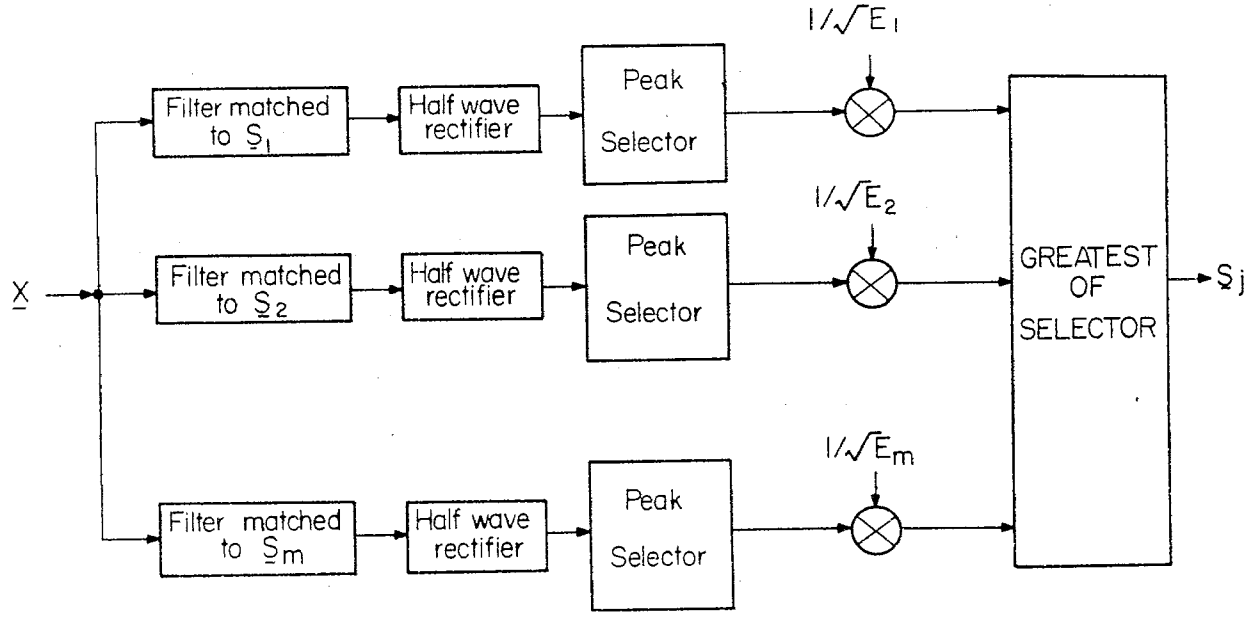

FIG. 24 Likelihood discriminator for arbitrary positive signal amplitude and delay.

SECTION 7

REFERENCES

1. C.L. Bennett, J.D. DeLorenzo and A.M. Auckenthaler, "Integral Equation Approach to Wideband Inverse Scattering," Volume I: Development of Procedures for Numerical Solution and Volume II: Computer Program Descriptions and Listings, Interaction Notes 226 and 227, June 1970.

2. C. L. Bennett, W. L. Weeks, "A Technique for Computing Approximate Electromagnetic Impulse Response of Conducting Bodies, Interaction Note 222, June 1968.
3. J. D. DeLorenzo, Electromagnetic Transient Studies in Space-Time, Ph.D. Thesis, Graduate School, Boston University, May 1970.
4. Davenport and Root, An Introduction to Random Signals and Noise, Chapter 14 (McGraw-Hill Book Co., Inc., 1968), pp. 312-359.
5. Hancock and Wintz, Signal Detector Theory, Chapter 3 (McGraw-Hill Book Co., Inc., 1966), pp. 30-87.
6. Middleton, D., An Introduction to Statistical Communication Theory (McGraw-Hill Book Co., Inc., 1960).
7. W. L. Root, "An Introduction to the Theory at the Detection of Signals in Noise," Proc. IEEE 58, 610-622 (May 1970).
8. Davenport and Root, An Introduction to Random Signals and Noise, Chapter 8 (McGraw-Hill Book Co., Inc., 1958), pp. 145-170.

APPENDIX A

BAND-LIMITED CORRELATION MATRICES

This appendix contains the matrices used in the bandwidth study in Sec. 3. The Bargraph in Fig. 16 was computed from the data contained here.

	SPHERE	CUBE		FLAT END CYLINDER				SPHERE CAPPED CYLINDER				RECTANGULAR CYLINDER				SPHERE-CONE-SPHERE							
		0*	45*	0*	30*	60*	90*	0*	30*	60*	90*	0*	30*	60*	90*	0*	30*	60*	90*	120*	150*	180*	
SPHERE	1.00	-.526	.665	-.460	.749	.902	.603	-.466	.432	.920	.614	.508	-.435	.830	.584	.840	.849	.914	.920	.937	.831	.729	
CUBE		1.00	.552	.841	.575	.632	.868	.785	.696	.606	.835	.875	.731	.602	.904	.709	.757	.596	.717	-.664	-.684	-.660	0*
			1.00	-.485	.749	.639	-.618	.625	.570	.627	-.633	-.514	.664	.675	-.510	.684	.672	.643	.662	.678	.481	-.420	45*
FLAT END CYLINDER				1.00	.668	.613	.762	.582	-.555	.538	.740	.974	.639	-.492	.824	.520	.620	.434	.618	-.605	-.639	-.615	0*
					1.00	.829	.627	-.502	.541	.702	.643	.673	-.444	.646	.585	.565	.638	.645	.749	.713	.558	-.500	30*
						1.00	.662	.550	-.444	.858	.687	.662	.503	.719	.715	.812	.830	.809	.919	.788	.674	-.610	60*
							1.00	.694	.659	.699	.979	.797	.624	.606	.811	.790	.764	.622	.809	-.712	.715	.700	90*
SPHERE CAPPED CYLINDER								1.00	.769	.535	.741	.577	.913	.496	.701	.595	.636	.491	.629	-.590	-.601	-.571	0*
									1.00	-.412	.657	-.510	.698	.739	.622	.596	.616	.607	.515	.540	-.524	-.502	30*
										1.00	.729	.588	.516	.694	.694	.813	.824	.768	.920	.848	.892	.830	60*
											1.00	.762	.675	.617	.778	.782	.796	.609	.835	-.721	-.686	.704	90*
RECTANGULAR CYLINDER												1.00	.636	-.486	.812	.624	.685	.508	.690	-.636	-.655	-.637	0*
													1.00	.389	.586	.618	.659	.458	.614	-.562	-.557	-.540	30*
														1.00	.592	.788	.830	.881	.786	.810	.638	.559	60*
															1.00	.634	.695	.550	.726	-.650	-.658	.671	90*
SPHERE CONE SPHERE																1.00	.937	.912	.921	-.681	.665	.614	0*
																	1.00	.899	.931	.664	.630	.592	30*
																		1.00	.871	.825	.636	.530	60*
																			1.00	.772	.723	.668	90*
																				1.00	.879	.799	120*
																					1.00	.948	150*
																						1.00	180*

FIG. A-1 Correlation matrix of target responses over the bandwidth 0-4.8 GHz with the specular return removed.

SPHERE	CUBE		FLAT END CYLINDER				SPHERE CAPPED CYLINDER				RECTANGULAR CYLINDER				SPHERE-CONE-SPHERE							
	0*	45*	0*	30*	60*	90*	0*	30*	60*	90*	0*	30*	60*	90*	0*	30*	60*	90*	120*	150*	180*	
1.00	-.530	.664	-.462	.741	.891	.605	-.462	.428	.912	.609	.515	-.435	.827	.588	.835	.842	.911	.917	.934	.820	.722	SPHERE
	1.00	.556	.840	.569	.634	.864	.776	.687	.610	.828	.876	.733	.593	.905	.716	.762	.681	.723	-.665	-.676	-.658	0*
		1.00	-.486	.746	.630	-.615	.612	.570	.622	-.629	-.518	-.658	.665	-.511	.681	.673	.644	.658	.669	.469	-.414	45* CUBE
			1.00	.666	.613	.758	.572	-.553	.537	.738	.969	.638	-.490	.823	.523	.621	.433	.618	-.605	-.630	-.612	0*
				1.00	.821	.623	-.503	.529	.696	.641	.669	-.442	.632	.581	.554	.629	.633	.742	.704	.550	-.491	30*
					1.00	.655	.532	-.438	.850	.679	.662	.492	.707	.716	.804	.818	.797	.911	.783	.662	-.602	60* FLAT END CYLINDER
						1.00	.684	.654	.698	.975	.796	.622	.601	.809	.791	.763	.624	.811	-.709	.709	.696	90*
							1.00	.770	.519	.737	.565	.899	.488	.700	.587	.622	.487	.616	-.581	-.587	-.561	0*
								1.00	-.408	.649	-.503	.699	.727	.616	.595	.606	.597	.512	.529	-.511	-.496	30* SPHERE CAPPED
									1.00	.724	.591	.506	.679	.695	.889	.815	.760	.914	.842	.875	.822	60* CYLINDER
										1.00	.759	.674	.613	.774	.777	.790	.604	.831	-.718	-.674	.698	90*
											1.00	.632	-.483	.814	.632	.690	.513	.695	-.637	-.648	-.635	0*
												1.00	-.384	.587	.615	.654	.452	.610	-.558	-.548	-.535	30*
													1.00	.589	.783	.823	.876	.782	.803	.626	.550	60* RECTANGULAR CYLINDER
														1.00	.640	.698	.552	.732	-.650	-.649	.666	90*
															1.00	.931	.909	.918	-.677	.656	.611	0*
																1.00	.895	.927	.661	.619	.586	30*
																	1.00	.867	.819	.628	.523	60*
																		1.00	.770	.713	.664	90* SPHERE CONE SPHERE
																			1.00	.866	.791	120*
																				1.00	.916	150*
																					1.00	180*

FIG. A-2 Correlation matrix of target responses with specular return removed.

SPHERE	CUBE		FLAT END CYLINDER				SPHERE CAPPED CYLINDER				RECTANGULAR CYLINDER				SPHERE-CONE-SPHERE								
	0*	45*	0*	30*	60*	90*	0*	30*	60*	90*	0*	30*	60*	90*	0*	30*	60*	90*	120*	150*	180*		
1.00	.686	.812	.558	.836	.944	.725	.608	.663	.937	.738	.608	.647	.904	.641	.926	.930	.954	.963	.582	.548	.494		SPHERE
	1.00	.687	.870	.667	.682	.889	.858	.820	.692	.891	.921	.766	.786	.924	.781	.797	.762	.735	.516	.373	.395	0*	CUBE
		1.00	.615	.676	.786	.610	.600	.598	.749	.622	.676	.741	.762	.535	.828	.876	.854	.811	.689	.504	-.518	45*	
			1.00	.666	.578	.823	.705	.572	.601	.785	.967	.774	.601	.865	.621	.631	.573	.580	.333	.376	.408	0*	
				1.00	.888	.748	.570	.575	.803	.769	.701	.583	.689	.616	.716	.743	.736	.796	.415	.443	.383	30*	FLAT END
					1.00	.770	.650	.668	.920	.788	.631	.708	.822	.599	.900	.916	.895	.953	.483	.468	.480	60*	CYLINDER
						1.00	.805	.797	.783	.985	.842	.782	.772	.881	.820	.810	.745	.886	-.464	-.425	.443	90*	
							1.00	.841	.675	.832	.735	.858	.695	.764	.753	.759	.715	.694	.606	-.367	.374	0*	
								1.00	.632	.807	.639	.683	.848	.750	.772	.774	.791	.722	.555	.378	.393	30*	SPHERE CAPPED
									1.00	.810	.668	.708	.836	.681	.914	.907	.880	.945	.431	.572	.554	60*	CYLINDER
										1.00	.843	.800	.776	.846	.823	.813	.748	.827	-.462	-.447	.458	90*	
											1.00	.791	.660	.868	.674	.702	.629	.653	.337	.379	.392	0*	
												1.00	.661	.648	.801	.796	.730	.754	.596	.426	.442	30*	RECTANGULAR
													1.00	.756	.911	.914	.949	.906	.621	.473	.482	60*	CYLINDER
														1.00	.712	.699	.665	.666	-.404	.334	.407	90*	
															1.00	.986	.964	.965	.639	.526	.535	0*	
																1.00	.972	.970	.643	.516	.527	30*	
																	1.00	.945	.714	.513	.517	60*	
																		1.00	.571	.501	.516	90*	SPHERE CONE SPHERE
																			1.00	.682	.625	120*	
																				1.00	.753	150*	
																					1.00	180*	

FIG. A-3 Correlation matrix of target responses over the bandwidth 0-6.4 GHz.

SPHERE	CUBE		FLAT END CYLINDER				SPHERE CAPPED CYLINDER				RECTANGULAR CYLINDER				SPHERE-CONE-SPHERE							
	0*	45*	0*	30*	60*	90*	0*	30*	60*	90*	0*	30*	60*	90*	0*	30*	60*	90*	120*	150*	180*	
1.00	.687	.812	.559	.835	.944	.725	.609	.665	.937	.738	.609	.648	.906	.642	.927	.931	.955	.963	.582	.549	.491	SPHERE
	1.00	.687	.871	.668	.684	.889	.859	.821	.693	.892	.921	.766	.788	.924	.782	.798	.764	.736	.517	.371	.397	0* CUBE
		1.00	.615	.677	.786	.610	.600	.597	.749	.621	.676	.743	.763	.535	.828	.875	.854	.812	.668	.503	-.519	45*
			1.00	.667	.578	.823	.706	.573	.601	.784	.967	.774	.601	.864	.622	.632	.574	.581	.334	.377	.407	0*
				1.00	.888	.748	.570	.577	.802	.769	.782	.583	.690	.616	.716	.744	.737	.796	.416	.443	.384	30* FLAT END
					1.00	.770	.650	.671	.921	.789	.631	.709	.823	.600	.901	.917	.896	.954	.483	.469	.481	60* CYLINDER
						1.00	.806	.797	.782	.985	.842	.781	.772	.881	.820	.811	.746	.806	-.465	-.427	.445	90*
							1.00	.843	.676	.831	.735	.858	.694	.764	.753	.760	.717	.694	.607	-.369	.374	0*
								1.00	.632	.807	.640	.684	.847	.750	.773	.775	.792	.723	.556	.377	.395	30* SPHERE CAPPED
									1.00	.810	.668	.710	.837	.681	.914	.908	.881	.945	.432	.578	.556	60* CYLINDER
										1.00	.843	.800	.775	.846	.823	.813	.749	.827	-.463	-.448	.452	90*
											1.00	.791	.661	.867	.675	.702	.630	.654	.338	.380	.392	0*
												1.00	.662	.648	.801	.797	.732	.755	.598	.426	.444	30* RECTANGULAR
													1.00	.757	.912	.915	.950	.906	.621	.472	.483	60* CYLINDER
														1.00	.713	.699	.666	.666	-.404	.335	.418	90*
															1.00	.986	.965	.966	.638	.525	.536	0*
																1.00	.972	.970	.643	.515	.527	30*
																	1.00	.946	.714	.512	.518	60* SPHERE
																		1.00	.571	.501	.517	90* CONE SPHERE
																			1.00	.682	.624	120*
																				1.00	.754	150*
																					1.00	180*

FIG. A-4 Correlation matrix of target responses over the bandwidth 0-4.8 GHz.

SPHERE	CUBE		FLAT END CYLINDER				SPHERE CAPPED CYLINDER				RECTANGULAR CYLINDER				SPHERE-CONE-SPHERE							
	0*	45*	0*	30*	60*	90*	0*	30*	60*	90*	0*	30*	60*	90*	0*	30*	60*	90*	120*	150*	180*	
1.00	.709	.811	-.577	.836	.945	.729	.612	.665	.938	.745	.630	.645	.906	.661	.926	.932	.955	.963	.583	.549	.497	SPHERE
	1.00	.713	.870	.695	.702	.896	.872	.839	.715	.899	.916	.794	.811	.920	.795	.818	.776	.761	.535	.386	.407	0* CUBE
		1.00	.632	.676	.785	.610	.602	.597	.748	.624	.697	.743	.761	.548	.826	.675	.853	.810	.689	.506	-.523	45*
			1.00	.694	.595	.819	.705	.586	.623	.787	.976	.791	.611	.856	.635	.653	.586	.607	.339	.371	.403	0*
				1.00	.889	.761	.572	.576	.804	.777	.724	.583	.689	.649	.716	.744	.737	.797	.416	.444	.384	30* FLAT END
					1.00	.780	.657	.673	.925	.800	.657	.708	.822	.624	.902	.917	.896	.955	.486	.472	.484	60* CYLINDER
						1.00	.809	.796	.792	.985	.847	.785	.772	.884	.827	.822	.758	.821	-.476	-.439	.453	90*
							1.00	.843	.677	.831	.739	.863	.693	.785	.753	.761	.715	.697	.610	-.374	.375	0*
								1.00	.632	.806	.646	.683	.849	.759	.776	.776	.795	.723	.561	.381	.396	30* SPHERE CAPPED
									1.00	.814	.684	.709	.837	.696	.916	.908	.882	.946	-.434	.578	.562	60* CYLINDER
										1.00	.845	.806	.777	.847	.833	.820	.756	.832	-.476	-.458	.459	90*
											1.00	.799	.674	.860	.681	.713	.634	.670	.341	.380	.394	0*
												1.00	.658	.668	.799	.795	.728	.754	.597	.431	.446	30* RECTANGULAR
													1.00	.772	.912	.913	.951	.985	.624	.477	.486	60* CYLINDER
														1.00	.739	.731	.689	.681	-.422	.331	.423	90*
															1.00	.987	.964	.966	.638	.531	.538	0*
																1.00	.972	.970	.643	.520	.531	30*
																	1.00	.946	.715	.517	.520	60* SPHERE
																		1.00	.572	.504	.526	90* CONE SPHERE
																			1.00	.686	.625	120*
																				1.00	.756	150*
																					1.00	180*

FIG. A-5 Correlation matrix of target responses over the bandwidth 0-3.2 GHz.

	SPHERE	CUBE		FLAT END CYLINDER				SPHERE CAPPED CYLINDER				RECTANGULAR CYLINDER				SPHERE-CONE-SPHERE							
		0*	45*	0*	30*	60*	90*	0*	30*	60*	90*	0*	30*	60*	90*	0*	30*	60*	90*	120*	150*	180*	
SPHERE	1.00	.730	.790	.600	.843	.947	.733	.561	.620	.936	.734	.631	.621	.913	.719	.918	.928	.954	.959	.625	.616	-.557	
CUBE		1.00	.794	.837	.680	.790	.881	.874	.866	.754	.881	.865	.894	.817	.892	.869	.889	.835	.833	.562	.491	.499	0*
			1.00	.735	.671	.775	-.656	.625	.548	.723	-.709	.759	.758	.739	.623	.813	.870	.841	.786	.663	.514	-.577	45*
FLAT END CYLINDER				1.00	.711	.713	.770	.643	.524	.670	.763	.995	.825	.583	.770	.660	.710	.611	.683	-.319	.405	-.418	0*
					1.00	.912	.755	.459	.569	.796	.759	.726	.551	.719	.600	.722	.753	.765	.823	-.405	.482	-.437	30*
						1.00	.834	.660	.663	.941	.838	.739	.701	.839	.755	.905	.925	.902	.960	.516	-.536	-.498	60*
							1.00	.753	.763	.814	.987	.801	.798	.754	.835	.861	.858	.761	.881	-.529	-.584	-.574	90*
SPHERE CAPPED CYLINDER								1.00	.841	.657	.787	.662	.926	.633	.757	.747	.744	.686	.698	.612	-.445	-.434	0*
									1.00	.574	.762	.564	.678	.825	.779	.750	.763	.776	.788	.623	-.488	.418	30*
										1.00	.817	.701	.700	.822	.813	.908	.903	.871	.946	-.518	.646	.647	60*
											1.00	.794	.820	.736	.818	.852	.835	.753	.871	-.548	-.597	-.583	90*
RECTANGULAR CYLINDER												1.00	.831	.621	.798	.695	.747	.647	.716	-.334	.411	-.438	0*
													1.00	.618	.733	.788	.791	.698	.752	.572	.459	.464	30*
														1.00	.811	.915	.926	.965	.918	.695	.508	-.559	60*
															1.00	.828	.823	.769	.793	-.431	.434	.583	90*
SPHERE CONE SPHERE																1.00	.987	.959	.971	.641	-.568	-.578	0*
																	1.00	.978	.971	.646	.539	.555	30*
																		1.00	.949	.748	.533	-.582	60*
																			1.00	.582	-.573	.536	90*
																				1.00	.742	.675	120*
																					1.00	.863	150*
																						1.00	180*

FIG. A-6 Correlation matrix of target responses over the bandwidth 0-1.6 GHz.

SPHERE	CUBE		FLAT END CYLINDER				SPHERE CAPPED CYLINDER				RECTANGULAR CYLINDER				SPHERE-CONE-SPHERE							
	0*	45*	0*	30*	60*	90*	0*	30*	60*	90*	0*	30*	60*	90*	0*	30*	60*	90*	120*	150*	180*	
1.00	.719	.867	-.699	.845	.945	.765	.587	.650	.943	.770	.675	.631	.889	.694	.927	.933	.958	.959	.619	.731	.676	SPHERE
	1.00	.738	.876	.699	.703	.917	.667	.832	.728	.922	.921	.784	.819	.936	.794	.824	.786	.766	.556	.493	.473	0*
		1.00	-.735	.771	.852	.733	-.629	.587	.859	.751	.773	.738	.777	.645	.844	.884	.854	.860	.524	.644	.597	45* CUBE
			1.00	.719	-.625	.836	.711	.587	.661	.811	.976	.801	-.648	.865	.658	.685	-.684	-.656	.381	.435	.457	0*
				1.00	.890	.755	.556	.563	.792	.769	.744	.588	.678	.645	.712	.755	.752	.792	-.533	.504	.572	30*
					1.00	.795	.637	.658	.923	.811	.684	.701	.797	.633	.895	.917	.901	.948	.573	.685	.640	60* FLAT END CYLINDER
						1.00	.817	.811	.798	.986	.861	.813	.885	.884	.865	.870	.812	.846	-.592	.555	.523	90*
							1.00	.833	.668	.844	.743	.856	.671	.791	.738	.750	.704	.678	.656	.474	.451	0*
								1.00	.625	.822	.645	.661	.847	.771	.762	.764	.793	.708	.570	.492	.468	30* SPHERE CAPPED
									1.00	.815	.719	.728	.830	.706	.935	.941	.910	.949	.598	.789	.652	60* CYLINDER
										1.00	.866	.838	.803	.847	.868	.866	.812	.854	-.568	.557	.523	90*
											1.00	.807	.706	.867	.704	.747	.676	.701	.380	.458	.458	0*
												1.00	.634	.685	.789	.785	.711	.754	.591	.540	.510	30*
													1.00	.807	.902	.907	.948	.890	.583	.671	.622	RECTANGULAR 60* CYLINDER
														1.00	.770	.772	.745	.782	-.545	.493	.465	90*
															1.00	.985	.966	.968	.606	.739	.684	0*
																1.00	.971	.979	.586	.727	.673	30*
																	1.00	.949	.649	.732	.677	60*
																		1.00	.615	.745	.690	SPHERE 90* CONE
																			1.00	.524	-.541	SPHERE 120*
																				1.00	.666	150*
																					1.00	180*

FIG. A-7 Correlation matrix of target responses over the bandwidth 0.5-3.2 GHz.

SPHERE	CUBE		FLAT END CYLINDER				SPHERE CAPPED CYLINDER				RECTANGULAR CYLINDER				SPHERE-CONE-SPHERE							
	0*	45*	0*	30*	60*	90*	0*	30*	60*	90*	0*	30*	60*	90*	0*	30*	60*	90*	120*	150*	180*	
1.00	.860	.962	-.794	.904	.952	.946	.749	.789	.947	.945	.839	.820	.864	.772	.947	.963	.957	.968	.634	.651	.737	SPHERE
	1.00	.806	.872	.743	.752	.937	.856	.833	.857	.939	.922	.768	.885	.944	.884	.896	.887	.847	.721	.692	.699	0*
		1.00	-.794	.891	.952	.878	.687	.711	.948	.888	.850	.809	.803	-.695	.881	.928	.902	.919	.534	.625	.691	45* CUBE
			1.00	.778	-.716	.836	.692	-.593	.779	.805	.973	.812	-.738	.867	-.758	-.787	-.771	-.788	.571	.548	.763	0*
				1.00	.915	.820	.625	.585	.856	.849	.812	.719	.659	.644	.755	.884	.769	.849	-.577	-.576	.694	30*
					1.00	.847	.703	.703	.923	.875	.749	.798	.727	-.618	.876	.989	.884	.941	.553	.618	.686	60* FLAT END CYLINDER
						1.00	.820	.840	.915	.982	.866	.793	.903	.882	.940	.938	.938	.919	-.705	.698	.743	90*
							1.00	.812	.850	.839	.732	.828	.755	.818	.857	.845	.829	.778	.849	.689	.563	0*
								1.00	.784	.850	.661	.647	.928	.795	.869	.874	.904	.815	-.716	.688	.563	30* SPHERE
									1.00	.942	.848	.890	.814	.746	.928	.947	.923	.937	.705	.654	.698	60* CAPPED CYLINDER
										1.00	.870	.813	.890	.837	.938	.958	.944	.949	.714	.679	.738	90*
											1.00	.808	.788	.864	.780	.814	.789	.785	.554	.541	.761	0*
												1.00	.698	.679	.851	.827	.823	.819	.777	-.639	.728	30*
													1.00	.854	.897	.895	.928	.867	-.647	.618	.681	60* RECTANGULAR CYLINDER
														1.00	.792	-.783	.795	.716	-.698	.669	.638	90*
															1.00	.980	.985	.956	.811	.684	.680	0*
																1.00	.998	.977	.748	.664	.695	30*
																	1.00	.962	.746	.660	.702	60*
																		1.00	.713	.671	.717	90* SPHERE CONE SPHERE
																			1.00	-.738	.493	120*
																				1.00	.436	150*
																					1.00	180*

FIG. A-8 Correlation matrix of target responses over the bandwidth 0.9-3.2 GHz.

SPHERE	CUBE		FLAT END CYLINDER				SPHERE CAPPED CYLINDER				RECTANGULAR CYLINDER				SPHERE-CONE-SPHERE								
	0*	45*	0*	30*	60*	90*	0*	30*	60*	90*	0*	30*	60*	90*	0*	30*	60*	90*	120*	150*	180*		
1.00	.923	.975	.885	.915	.928	.922	.952	.871	.943	.933	.929	.873	.905	.925	.972	.955	.961	.983	.949	.854	.783		SPHERE
	1.00	.943	.946	.789	.838	.937	.912	.871	.887	.958	.985	-.831	.886	.981	.923	.894	.922	.919	.885	.807	.822	0*	CUBE
		1.00	.905	.867	.913	.919	.931	.902	.929	.948	.947	.884	.932	.937	.979	.950	.969	.966	.919	.860	.782	45*	
			1.00	.716	.812	.952	.846	.878	.869	.949	.949	-.860	.917	.954	.907	.909	.919	.896	.893	.879	.814	0*	
				1.00	.892	-.835	.932	.814	.890	.834	.770	.736	.782	.816	.892	.890	.870	.877	.888	.737	.618	30*	
					1.00	-.834	.860	.803	.809	.834	.812	.771	.806	.837	.899	.906	.878	.912	.849	.828	.666	60*	FLAT END CYLINDER
						1.00	.924	.940	.958	.984	.948	.822	.953	.966	.935	.952	.948	.940	.930	.833	.816	90*	
							1.00	.862	.944	.939	.892	.762	.877	.931	.948	.938	.937	.929	.929	.772	.763	0*	
								1.00	.934	.941	.878	.827	.920	.918	.930	.930	.953	.892	.854	.776	.722	30*	SPHERE CAPPED
									1.00	.935	.906	.867	.921	.900	.937	.954	.940	.948	.927	.804	.766	60*	CYLINDER
										1.00	.953	-.821	.934	.984	.964	.959	.971	.919	.914	.833	.797	90*	
											1.00	.878	.922	.966	.930	.904	.930	.936	.897	.848	.840	0*	
												1.00	.867	-.827	.875	.856	.886	.887	.861	.862	-.728	30*	
													1.00	.883	.907	.924	.920	.923	.914	.814	.820	60*	RECTANGULAR CYLINDER
														1.00	.945	.937	.954	.898	.885	.822	.802	90*	
															1.00	.981	.988	.948	.909	.868	.743	0*	
																1.00	.982	.979	.931	.863	.792	30*	
																	1.00	.940	.901	.850	.778	60*	
																		1.00	.948	.872	.798	90*	SPHERE CONE SPHERE
																			1.00	.812	.801	120*	
																				1.00	-.628	150*	
																					1.00	180*	

FIG. A-9 Correlation matrix of target responses over the bandwidth 1.7-4.8 GHz.

APPENDIX B

GENERATION OF GAUSSIAN NOISE

A uniform random-number generator produces a sequence of numbers X_R, where

$$X_{n+1} = (11^3 \cdot X_n) \bmod 2^{11}$$

$$X_o = \text{any odd number.}$$

This sequence is then adjusted to have zero mean and the appropriate range

$$X_n = (2^{-11} X_n - \tfrac{1}{2})R$$

where

$$R = \text{range.}$$

The Gaussian random numbers are produced in steps. First, a uniform random-number generator generates a sequence of numbers X_n, where

$$X_{n+1} = (21^5 \cdot X_n) \bmod 2^{22}$$

where

$$X_o = \text{any odd number.}$$

Then a sequence Y_n is formed such that

$$Y_n = \sum_{k=1}^{12} (2^{-22} X_k - \tfrac{1}{2})$$

which is approximately Gaussian with unit variance.